



AMERICAN UNIVERSITY OF BEIRUT

SYNTHESIS AND STRUCTURAL EVOLUTION OF METAL-  
ORGANIC FRAMEWORKS BY REACTION-DIFFUSION  
PROCESS AT ROOM TEMPERATURE

by  
RAZAN MOHAMMAD ISSA

A thesis  
submitted in partial fulfillment of the requirements  
for the degree of Master of Science  
to the Department of Chemistry  
of the Faculty of Arts and Sciences  
at the American University of Beirut

Beirut, Lebanon  
July 2017

AMERICAN UNIVERSITY OF BEIRUT

SYNTHESIS AND STRUCTURAL EVOLUTION OF METAL-  
ORGANIC FRAMEWORKS BY REACTION-DIFFUSION  
PROCESS AT ROOM TEMPERATURE

by  
RAZAN MOHAMMAD ISSA

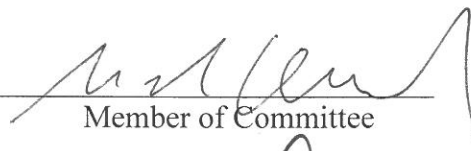
Approved by:



Dr. Mohamad Hmadeh, Assistant Professor  
Chemistry

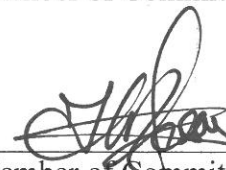
Advisor

Dr. Mazen Al-Ghoul, Professor  
Chemistry



Member of Committee

Dr. Houssam El-Rassy, Associate Professor  
Chemistry



Member of Committee

Dr. Digambara Patra, Associate Professor  
Chemistry



Member of Committee

Date of thesis defense: July 13, 2017

# AMERICAN UNIVERSITY OF BEIRUT

## THESIS, DISSERTATION, PROJECT RELEASE FORM

Student Name: \_\_\_\_\_  
Last First Middle

Master's Thesis       Master's Project       Doctoral Dissertation

I authorize the American University of Beirut to: (a) reproduce hard or electronic copies of my thesis, dissertation, or project; (b) include such copies in the archives and digital repositories of the University; and (c) make freely available such copies to third parties for research or educational purposes.

I authorize the American University of Beirut, to: (a) reproduce hard or electronic copies of it; (b) include such copies in the archives and digital repositories of the University; and (c) make freely available such copies to third parties for research or educational purposes

after:

**One --- year from the date of submission of my thesis, dissertation, or project.**

**Two --- years from the date of submission of my thesis, dissertation, or project.**

**Three --- years from the date of submission of my thesis, dissertation, or project.**

---

Signature

Date

## ACKNOWLEDGEMENTS

First of all, I would candidly like to dedicate my deepest gratitude to my advisor Dr. Mohamad Hmadeh and Co-advisor Dr. Mazen Al-Ghoul for their unwavering guidance, support and patience. I am extremely thankful and grateful to them for their vast expert, sincere guidance and mentorship. Thank you for providing me with all the crucial facilities, through which I was able to complete this thesis.

I would like to express my gratefulness to the committee members Dr. Houssam El-Rassy and Dr. Digambara Patra for their supervision on this thesis.

I place on record my genuine gratitude to the CRSL members, Dr. Mneimneh, Juan and Rania for their immense technical assistance.

I would like to outspread my thanks to all the graduate students for their collegial assistance over the few years. Special thanks to Manal, Hala, Mahmoud, Mira, Antranik, Mazhar, Maya and Sandrine.

I take this chance to acknowledge all the faculty members of the Department of Chemistry for their valuable help and support in this venture.

Finally, I would like to dedicate this thesis to my beloved family. Thank you for having the faith in me and for your unceasing encouragement.

## AN ABSTRACT OF THE THESIS

Razan Mohammad Issa for Master of Science  
Major: Chemistry

Title: Synthesis and structural evolution of metal-organic frameworks (MOFs) by reaction-diffusion process at room temperature

Metal organic Frameworks (MOFs) are new class of hybrid materials that are composed of organic linkers and inorganic clusters joined via strong bonds. MOFs have been mainly synthesized via solvothermal, sonochemical, mechanochemical, fast precipitation or slow diffusion techniques. Herein, we report for the first time the synthesis of metal-organic frameworks (MOFs) via a reaction-diffusion process at room temperature. Our novel synthesis system is based on the separation of the reactants by immobilizing the organic linker in a gel matrix and the metal salt solution is added on the top of the gel and allowed to diffuse through the inner electrolyte forming thereby the corresponding MOF crystals. As a proof of concept, MOF-199 structure is considered in this study and it was successfully synthesized via this method. MOF-199 (also known as HKUST-1) was chosen because it is one of the most prominent MOFs due to its considerable high surface area, large pore volume, high thermal and chemical stability especially in water. Beside its novelty, this method is rapid, efficient, scalable, and environmentally friendly. Additionally, it allows us to adjust and control the size distribution and the morphology of the particles. The obtained crystals were subjected to characterization using different instruments and techniques such as XRD, SEM, TGA, BET, FT-IR and  $^1\text{H-NMR}$ . Furthermore, different experimental conditions were varied in order to examine their effect on the size and the morphology of the MOF crystals. Such conditions include temperature, concentration of the inner, source of the metal in the outer, concentration of the gel and its type. Another discovered advantage of this method was the successful incorporation of two different linkers within the same framework in a controlled manner. Finally, the adsorption performance over methylene blue of MOF-199 was compared to that of mixed-linkers MOF and showed a great enhancement due to the heterogeneity within order introduced in the crystals.

# CONTENTS

	Page
ACKNOWLEDGEMENTS .....	V
ABSTRACT .....	vi
LIST OF ILLUSTRATIONS .....	xi
LIST OF TABLES .....	xv

## Chapter

I. INTRODUCTION.....	1
A. Metal-Organic Frameworks (MOFs) .....	1
1. Historical Background .....	1
2. Crystal Structure and Properties .....	3
3. Synthesis Routes of MOFs .....	8
a. Solvothermal Synthesis .....	9
b. Mechanochemical Synthesis .....	9
c. Slow-Evaporation Synthesis .....	10
d. Microwave Assisted Synthesis.....	10
e. Electrochemical Synthesis.....	11
f. Sonochemical Synthesis .....	11
4. Applications of MOFs.....	12
a. Gas Storage.....	14
b. MOFs as catalysts .....	13
c. MOFs as sensors.....	14
d. MOFs in drug delivery .....	16
e. Water Purification .....	17
B. Reaction-Diffusion Framework (RDF).....	18

1. RDF in Nature .....	18
2. RDF in Chemistry .....	20
a. Diffusion.....	20
b. Nucleation and Supersaturation .....	21
c. Crystal Growth .....	23
C. Objectives.....	23
<b>II. MOF-199 SINGLE CRYSTALS VIA REACTION- DIFFUSION FRAMEWORK: SYNTHESIS PROCEDURE AND CHARACTERIZATION .....</b>	<b>26</b>
A. Materials and Methods .....	26
1. Materials .....	26
2. Preparation of MOF-199 Single Crystals .....	26
B. Characterization of MOF-199 Single Crystals .....	27
1. Powder X-ray Diffraction (PXRD) .....	28
2. Scanning Electron Microscopy Analysis (SEM) .....	28
3. Nitrogen Adsorption and BET Calculation .....	28
4. Thermal Gravimetric Analysis .....	29
C. Results and Discussion.....	29
1. Powder X-ray diffraction (PXRD) patterns of the obtained MOF-199 by RDF .....	29
2. Determining the morphology of the MOF-199 single crystals.....	30
3. The surface area of MOF-199 synthesized via RDF .....	31
4. Thermal Stability of the obtained MOF-199.....	32
5. Yield of MOF-199 synthesized by RDF.....	33
6. Size and morphology control of MOF-199 single crystals .....	34
a. Effect of temperature.....	34
b. Inner Concentration [BTC] .....	36



c. Concentration of agar gel .....	38
d. Copper source of the outer .....	40
e. Type of the gel used in the inner .....	42
f. Reversing the components of the inner and the outer.....	48
7. Kinetic study and particle size analysis of MOF-199 .....	49
<b>III. SYNTHESIS OF MULTIVARIATE MOFS VIA RDF .....</b>	<b>53</b>
A. Materials and Methods.....	54
1. Materials .....	54
2. Preparation of the mixed linkers MOF and characterization .....	54
B. Results and Discussion .....	54
1. Influence of the variation of the proportion of the linkers BTC and 5-Hydroxyisophthalic acid on the purity of the obtained MOF .....	55
2. Effect of varying the ratios of the linkers on the surface area and the morphology of the MOF .....	56
3. Thermal Stability of the Mixed Linkers MOF .....	59
4. <sup>1</sup> H-NMR Analysis of the mixed linkers .....	60
<b>IV. ADSORPTION OF METHYLENE BLUE ON MOF-199 AND MIXED-LINKER MOFs .....</b>	<b>63</b>
A. Experimental Preparation.....	65
B. Results and Discussion.....	66
1. Effect of the initial pH of the solution.....	66
2. Thermodynamic Study: Effect of temperature.....	67
3. Type of adsorption isotherm.....	69
4. Kinetic Study .....	70
a. Adsorption Mechanism: Intra-particle diffusion.....	71
b. Activation Energy .....	72
<b>V. CONCLUSION AND FUTURE WORK.....</b>	<b>75</b>

A. Conclusion .....	75
B. Future Work .....	76
1. Synthesis of new MOFs via RDF.....	76
2. Synthesis of other mixed-metals MOFs via RDF .....	77
3. Synthesis of other mixed-linkers MOFs.....	78
<b>REFERENCES .....</b>	<b>79</b>

# ILLUSTRATIONS

Figure	Page
1. 1. Crystal structure of (A) MOF-199, (B) MOF-5. The yellow sphere in the middle describes the cavity without contacting the Van der Waals of the interior atoms. Reprinted with permission from ref. [7]. Copyright 1999 Nature. ....	2
1. 2. Number of publications on the topic of “Metal-Organic Frameworks” per year. Reprinted with permission from ref. [12]. Copyright 2014 Royal Society of Chemistry.....	2
1. 3. The metal ions and the organic linkers are the components making up the MOF structure. Reprinted with permission from ref. [17]. Copyright 2016 Nature. ....	4
1. 4. Development in the surface areas before and after the discovery of MOFs. Reprinted with permission from ref. [22]. Copyright 2013 Science. ....	4
1. 5. Crystal Structures of MOFs having high Brunauer-Emmett-Teller (BET) surface areas. Reprinted with permission from ref. [22]. Copyright 2013 Science. ....	5
1. 6. The prominent diversity of (A) metal clusters, (B) organic linkers incorporated in the synthesis of MOFs. Reprinted with permission from ref. [22]. Copyright 2013 Science. ....	6
1. 7. Crystal Structure of a series of IRMOFs and their corresponding functionalized ligand derivatives. $R_1 = -H$ , $R_2 = -Br$ , $R_3 = -NH_2$ , $R_4 = -O-CH_2-CH_2-CH_3$ , $R_5 = -O-CH_2-CH_2-CH_2-CH_2-CH_3$ , $R_6 = -C_4H_2$ , $R_7 = -C_6H_4$ . Reprinted with permission from ref. [11]. Copyright 2002 Science.....	7
1. 8. Schematic representation of the concept of multivariate MOFs (MTV-MOFs) using a variety of organic linkers. ....	8
1. 9. Illustrations of diverse animate (a-d) and inanimate (e-h) RDF systems on different length scales ( $\mu m$ , mm, m). Reprinted with permission from ref. [112]. Copyright 2009 John Wiley & Sons. ....	19
2. 1. (A) Schematic representation of the MOF-199 synthesis via RDF. (B) MOF-199 crystals formed after washing and drying. ....	27
2. 2. (A) Crystal structure of MOF-199. C, black; O, red; Cu, blue. Hydrogen atoms are removed for clarity. (B) PXRD patterns of MOF-199 crystals of (a) calculated one compared to (b) MOF-199 prepared via RDF. ....	30
2. 3. Optical microscope images showing the cubic morphology of the MOF-199 prepared by RDF method.....	31

2. 4. SEM images of MOF-199 taken at different scales.....	31
2. 5. Nitrogen physisorption isotherm of MOF-199 synthesized via RDF.....	32
2. 6. Thermogravimetric curves of MOF-199 under nitrogen atmosphere with a heating rate of 3°C.min <sup>-1</sup> and a temperature ranging from 30 °C to 700 °C of the as synthesized MOF-199 (red), activated MOF-199 (black). ....	33
2. 7. MOF-199 prepared via RDF process at different scales.....	34
2. 8. (A) Histogram showing the variation of the average particle size of MOF-199 (µm) as a function of temperature (°C). (B) Plot showing the average particle size (µm) in each band at different temperatures. ....	35
2. 9. SEM images showing the growth pattern of the MOF-199 particles at different temperatures and same inner concentration (10mM) in consecutive regions of the tube (0.5cm each). Scale bar 100 µm. ....	36
2. 10. (A) Histogram showing the variation of the average particle size (µm) of MOF-199 crystals at different inner concentrations [BTC]. (B) The variation of the average particle size (µm) of MOF-199 single crystals in each band as a function of the concentration of the inner [BTC].....	37
2. 11. SEM images showing the growth pattern of the MOF-199 particles at different inner [BTC] concentrations in consecutive regions of the tube (0.5cm each). Scale bar 100 µm. Scale bar 100 µm.....	38
2. 12. (A) Histogram showing the variation of the average particle size of MOF-199 crystals (µm) as a function of the agar gel concentration (%). (B) Plot showing the variation of the average particle size of MOF-199 crystals (µm) in each band as a function of the agar gel concentration (%). ....	39
2. 13. SEM images showing the growth pattern of the MOF-199 particles at different agar gel concentration in consecutive regions of the tube (0.5cm each). Scale bar 100 µm.....	40
2. 14. PXRD patterns of MOF-199 synthesized by RDF using different outer as compared to the theoretical one. (a) Calculated, (b) Cu(OAc) <sub>2</sub> .H <sub>2</sub> O in the outer, (c) Cu(NO <sub>3</sub> ) <sub>2</sub> .3H <sub>2</sub> O in the outer, (d) CuSO <sub>4</sub> .5H <sub>2</sub> O in the outer. ....	41
2. 15. SEM images of MOF-199 using different copper sources in the outer. (A) Cu(NO <sub>3</sub> ) <sub>2</sub> .3H <sub>2</sub> O, (B) CuSO <sub>4</sub> .5H <sub>2</sub> O. Microscopic images of MOF-199 using different copper sources in the outer. (C) Cu(NO <sub>3</sub> ) <sub>2</sub> .3H <sub>2</sub> O, (D) CuSO <sub>4</sub> .5H <sub>2</sub> O. .	42
2. 16. PXRD patterns of MOF-199 (a) calculated, (b) synthesized using LB Lennox agar gel.....	43

2. 17. SEM images of MOF-199 in organic gel taken at different consecutive positions from the interface. (1) Band 1, (2) Band 2, (3) Band 3, (4) Band 4, (5) Band 5. ..	44
2. 18. PXRD patterns of MOF-199 (a) calculated, (b) synthesized in DBS gel. ....	45
2. 19. SEM images of MOF-199 in organic gel taken at different consecutive positions from the interface. (1) Band 1, (2) Band 2, (3) Band 3, (4) Band 4, (5) Band 5. ..	46
2. 20. (A) SEM images of MOF-199 spheroids produced in organic gel after 1 min from adding the outer. (B) Histogram representing the average particle size of MOF-199 synthesized in organic gel and separated into five consecutive bands (0.5 cm each).....	47
2. 21. PXRD patterns of MOF-199 synthesized in organic gel. (a) The outer was kept, (b) the outer was discarded after 1 min from adding it to the inner. ....	48
2. 22. Microscopic and SEM images of the crystals of the system composed from Cu(OAc) <sub>2</sub> .H <sub>2</sub> O in the inner and BTC in the outer. ....	49
2. 23. PXRD patterns of (a) MOF-199 calculated, and (b)MOF sample under investigation.....	49
2. 24. SEM images of MOF-199 obtained after (A) 6 sec (B) 10 sec from adding the outer. ....	51
2. 25. PXRD patterns of (a) MOF-199 spheroids, (b) MOF-199 cubes. ....	51
3. 1. PXRD patterns of (a) MOF-199 calculated, mixed linkers MOF containing OH-BDC:BTC (b) 1:1, (c) 1:3, (d) 3:1. ....	56
3. 2. Nitrogen physisorption isotherms of the mixed-linker MOF with OH-BDC:BTC ratios (A) 1:3, (B) 1:1, (C) 3:1, (D) Histogram showing the surface area of MOF-199, OH-BDC:BTC (1:3), OH-BDC:BTC (1:1) and OH-BDC:BTC (3:1).....	57
3. 3. SEM images of the mixed-linkers MOFs obtained at different proportions. ....	58
3. 4. Thermogravimetric curves of MOF-199 and mixed-linker MOFs at different proportions under nitrogen atmosphere with a heating rate of 3°C.min <sup>-1</sup> and a temperature ranging from 30 °C to 860 °C.....	59
3. 5. FT-IR spectra of the mixed-linkers MOF at different ratios, BTC and 5-Hydroxyisophthalic acid. ....	60
3. 6. <sup>1</sup> H-NMR spectrum of mixed-linkers MOF OH-BDC:BTC.....	61
4. 1. Structure of Methylene Blue (MB).....	64

4. 2. Different adsorption mechanisms described for the adsorption of organic molecules on MOFs. ....	64
4. 3. (A) Effect of pH on the adsorption of Methylene Blue. (B) Percentage removal of Methylene Blue on the MOFs at different pHs. (Adsorption conditions: 10 mg of the MOF, 3.20 mg.L-1 of the dye, 120 min contact time and 298 K). ....	67
4. 4. (A) Van't Hoff plot for the adsorption of Methylene Blue on the MOF systems. (B) Percentage removal of Methylene Blue as a function of temperature for the MOF systems. ....	69
4. 5. Freundlich isotherm for Methylene Blue adsorption onto the four MOF systems.	70
4. 6. Plot of pseudo-second order kinetic models. ....	71
4. 7. Linear plot of intra-particle diffusion model for MOF-199, OH-BDC:BTC (1:1), OH-BDC:BTC (1:3) and OH-BDC:BTC (3:1). ....	72

## TABLES

Table	Page
3. 1. Table showing the mixed-linker MOFs prepared using different proportions of the organic linkers BTC and 5-Hydroxyisophthalic acid. ....	55
3. 2. Table showing the initial and the final amounts of the linkers OH-BDC and BTC incorporated in the MOF structure.....	62
4. 1. Thermodynamic parameters of methylene blue adsorption over adsorbents at different temperatures. ....	68
4. 2. Freundlich isotherm parameters for Methylene Blue adsorption on different MOF systems.....	70
4. 3. Correlation Coefficients of pseudo-first order and pseudo second-order kinetic models.....	71
4. 4. Kinetic parameters for the adsorption of Methylene Blue on the MOFs.....	73
4. 5. Freundlich constants for the adsorption of Methylene Blue by a series of adsorbents reported in literature. ....	74

# CHAPTER I

## INTRODUCTION

### **A. Metal-Organic Frameworks (MOFs)**

#### ***1. Historical Background***

In around 1990, the work of Hoskins and Robson concerning the formation of crystalline hybrid porous materials having efficient properties was considered the keystone for developing and shedding the light on porous coordination polymers. This work has shown a huge interest among scientists worldwide and was considered the base for the imminent progress of metal organic frameworks (MOFs)[1]. The term “Metal-Organic Frameworks” was foremost familiarized by Yaghi et al. in 1995[2], and it refers to a class of highly porous and crystalline materials composed of organic linkers and inorganic clusters connected via strong chemical bonds. In his paper, Yaghi introduced the synthesis of a thermally stable layered Cobalt-trimesate MOF having reversible sorption properties. After two years, Kitagawa et al. reported a 3D MOF displaying gas sorption properties[3]. Later on in 1999, two MOFs, MOF-5[4] and HKUST-1[5] were synthesized, and up till now they are still studied and considered the most important MOFs due to their remarkable stability and porosity[6], Fig. 1.1[7]. As the number of MOFs synthesized using single ligands has tremendously increased, the idea of preparing MOFs using mixed linkers started to appear by 2001[8]. By tuning these linkers, the dimensionality of the framework could be altered[9]. Early in 2002, Férey et al. introduced the concept of the flexibility of MOFs by designing several MOFs such as MIL-47, MIL-53, and MIL-88[10]. During the same year, Yaghi et al. popularized the concept of isoreticular chemistry through a series of zinc dicarboxylates



in addition to other extended dicarboxylate acids functionalized with different substituents such as methyl, amines, phenols, and thiols[11].

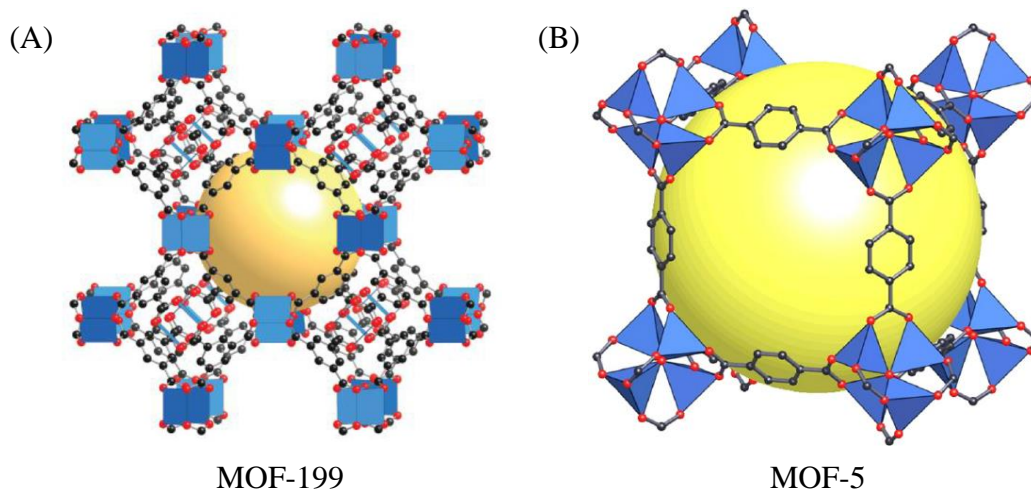


Figure 1. 1. Crystal structure of (A) MOF-199, (B) MOF-5. The yellow sphere in the middle describes the cavity without contacting the Van der Waals of the interior atoms. Reprinted with permission from ref. [7]. Copyright 1999 Nature.

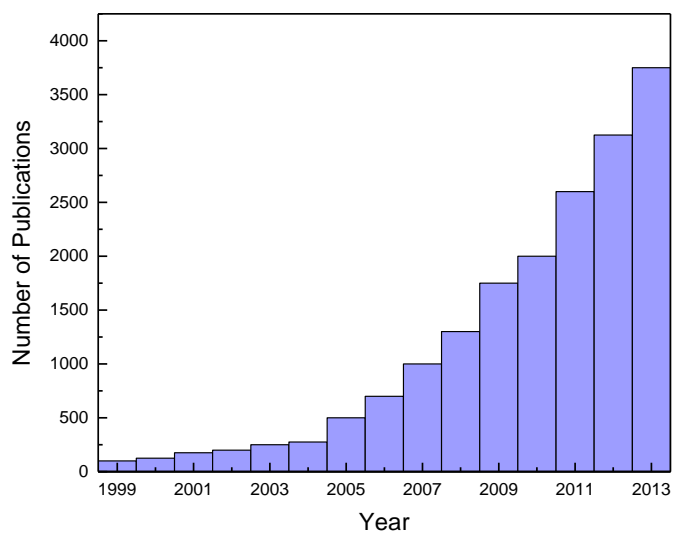


Figure 1. 2. Number of publications on the topic of “Metal-Organic Frameworks” per year. Reprinted with permission from ref. [12]. Copyright 2014 Royal Society of Chemistry.

## ***2. Crystal Structure and Properties***

Traditional materials such as zeolites and activated carbons suffer from the meagre connection between the reactants and products under certain reaction conditions, resulting in the collapse of their structure[12]. On the contrary, MOFs are a new class of highly crystalline porous extended frameworks characterized by their ultrahigh porosity, high surface area, flexibility[13] and good thermal stability overcoming zeolites and other ordinary porous materials[14]. These materials are characterized by their hybrid identity as they are formed by anchoring organic linkers mainly containing carboxylate moieties with metal clusters via strong coordination bonds[15] (Fig 1.3) [16]. The metal clusters in the framework are termed by secondary building units (SBUs), and their geometry is governed primarily by the coordination number of the metal[17]. Most of the metal centers making up the MOF structures are transition metals (e.g. Zinc, Cobalt and Copper) that act as Lewis acid acceptors due to the empty d orbitals, and receive electrons from the organic ligands to construct the coordination bonds[18]. As for the organic ligands, the benzene group functionalized with carboxylate moieties such as Terephthalic acid and 1,3,5-Benzenetricarboxylic acid, are considered the most extensively used linkers owing to their rigidity and propensity to generate firm metal-carboxylate clusters[19]. In addition to other organic linkers that form strong coordination bonds with the metal ions and contain atoms bearing electron lone pairs such as pyridine based derivatives[20].

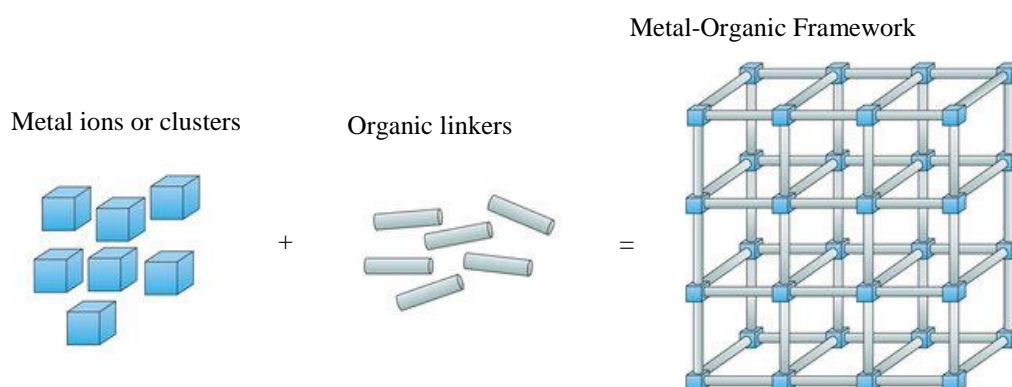


Figure 1. 3. The metal ions and the organic linkers are the components making up the MOF structure. Reprinted with permission from ref. [17]. Copyright 2016 Nature.

Another interesting feature that characterizes MOFs' structures is their ultrahigh surface area when compared to a variety of traditional porous materials (Fig. 1.4) [21]. Before the discovery of MOFs, the maximum surface area attained by the ordinary porous materials including zeolites, silicates and carbons was limited up to 1500 m<sup>2</sup>/g, whereas upon introducing MOFs the surface area increased dramatically and reached up to 7000 m<sup>2</sup>/g, Fig. 1.5[21].

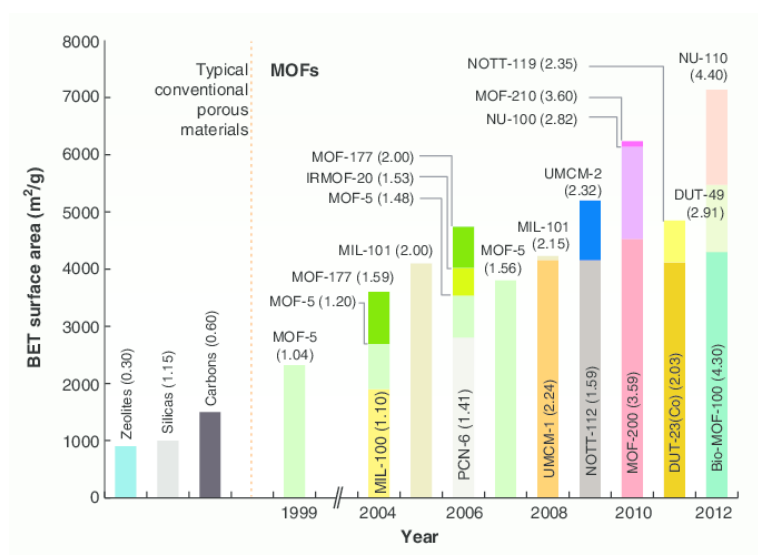


Figure 1. 4. Development in the surface areas before and after the discovery of MOFs. Reprinted with permission from ref. [22]. Copyright 2013 Science.

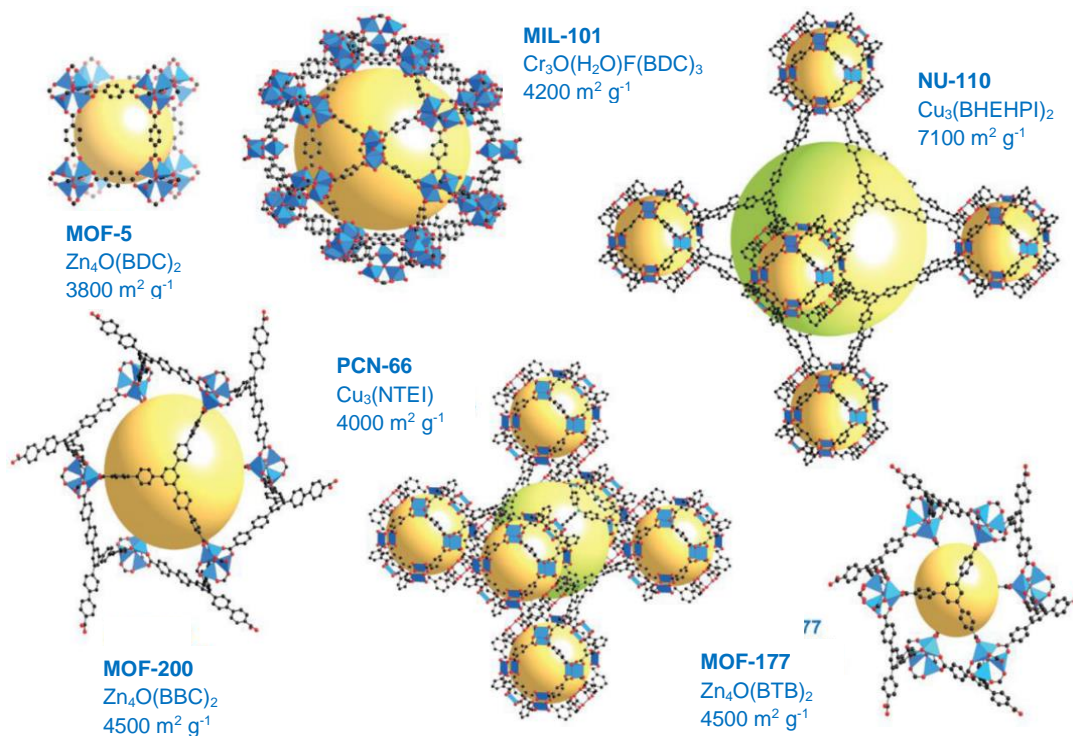


Figure 1. 5. Crystal Structures of MOFs having high Brunauer-Emmett-Teller (BET) surface areas. Reprinted with permission from ref. [22]. Copyright 2013 Science.

The conspicuous interest in MOFs does not rely back to their high surface areas only, but also to the immense number of metal salts and organic linkers that could be incorporated in the synthesis processes (Fig. 1.6)[21]. This variety in the choice of metal ions and organic linkers leads to a diversity of MOFs having different structures with altered properties and targeted for various applications including gas storage, separations and catalysis. In some cases, neither the crystal structure nor the properties of the MOF change upon varying the functionalities of the organic linkers, such types are called isorecticular MOFs (IRMOFs) as shown in Fig. 1.7[11].

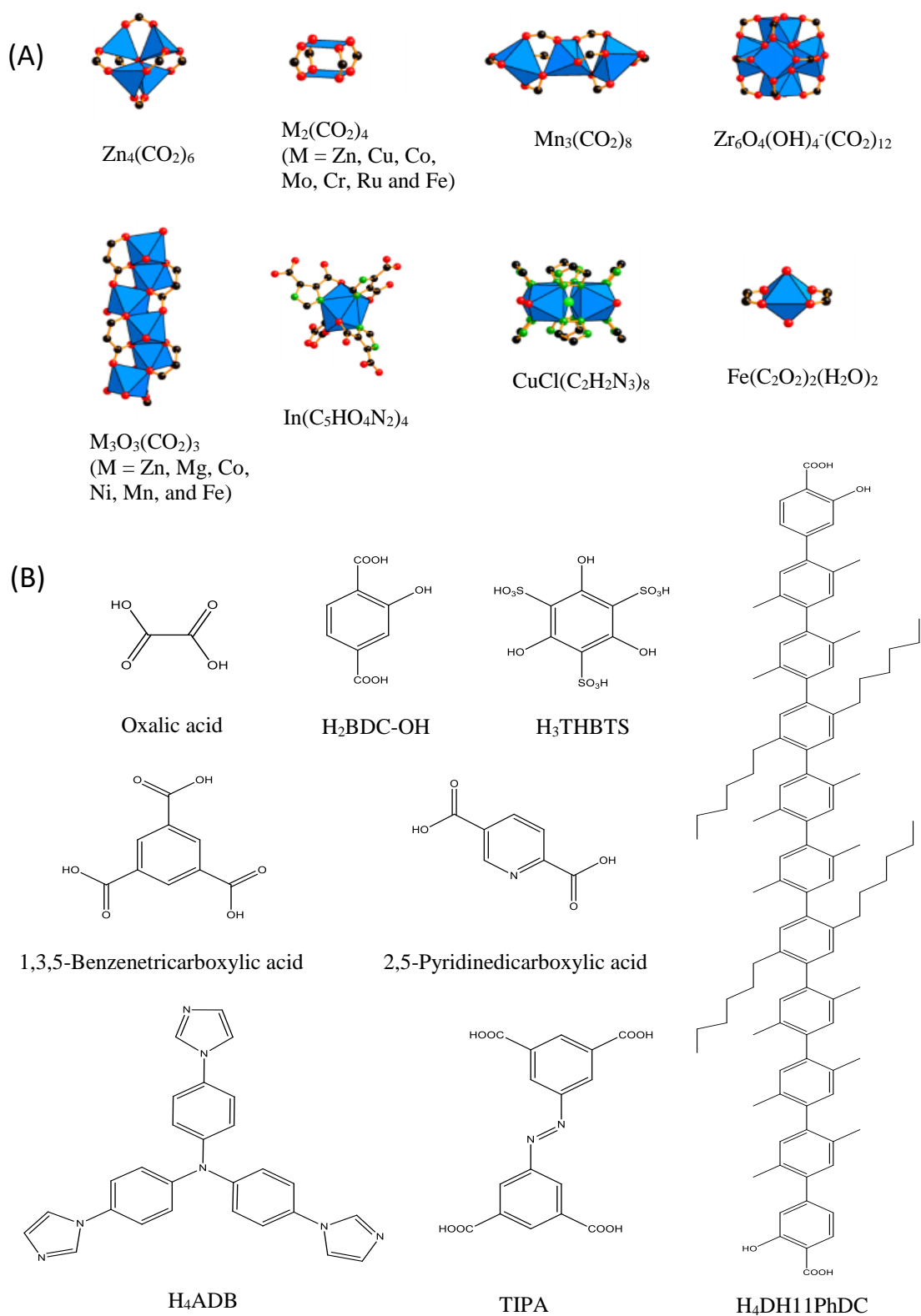


Figure 1. 6. The prominent diversity of (A) metal clusters, (B) organic linkers incorporated in the synthesis of MOFs. Reprinted with permission from ref. [22]. Copyright 2013 Science.

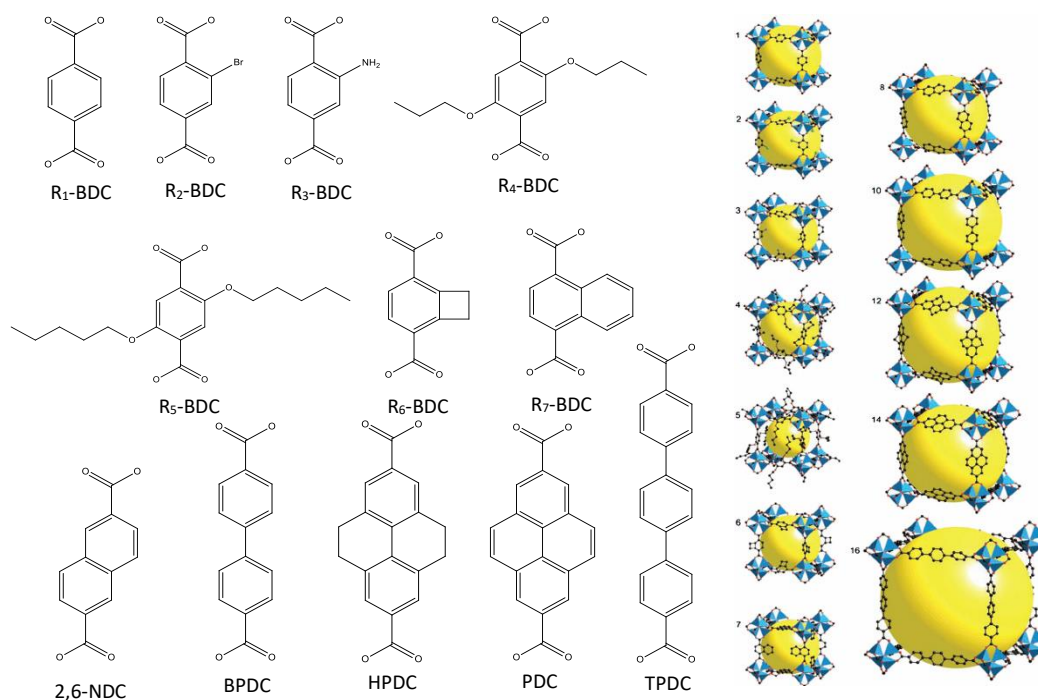


Figure 1. 7. Crystal Structure of a series of IRMOFs and their corresponding functionalized ligand derivatives.  $R_1 = -H$ ,  $R_2 = -Br$ ,  $R_3 = -NH_2$ ,  $R_4 = -O-CH_2-CH_2-CH_3$ ,  $R_5 = -O-CH_2-CH_2-CH_2-CH_2-CH_3$ ,  $R_6 = -C_4H_2$ ,  $R_7 = -C_6H_4$ . Reprinted with permission from ref. [11]. Copyright 2002 Science.

Furthermore, the properties of the MOFs including the porosity, flexibility and stability could be enhanced by incorporating more than one type of organic linker into the framework thereby inducing heterogeneity within the framework; such materials are known as multivariate MOFs (MTV-MOFs), Fig. 1.8[22, 23]. The intentions behind synthesizing MTV-MOFs is to generate versatile porous material that exclusively display dual opposing properties, creating defects while conserving the entire framework and adjust the pore environments via allocating the functional groups into the framework at the preferred locations[24]. All these schemes owe to influence the properties of the single ligand MOFs and thus enhance its performance on the application level[25]. However, this approach is considered challenging as the obtained material might lack a single phase of the mixed linkers or lose its crystalline order [26].

A conspicuous example of a mixed linker system is MOF-210 which is synthesized using the two organic linkers, the biphenyl-4,4'-dicarboxylate (BPDC) and the 4,4',4''-(benzene-1,3,5-triyl-tris(ethyne-2,1-diyl))tribenzoate (BTE) which exhibits two diverse kinds of pores with an outstandingly high surface area ( $6240 \text{ m}^2/\text{g}$ )[27]. Another example includes the synthesis of a series of mixed-linkers MOFs made from 1,4-Benzenedicarboxylic acid and 2-Amino-1,4-benzenedicarboxylic acid coordinated to zinc ions at different ratios. The concerned MOF is used as a catalyst for the synthesis of propylene carbonate from the reaction of propylene oxide and  $\text{CO}_2$  [23, 28].

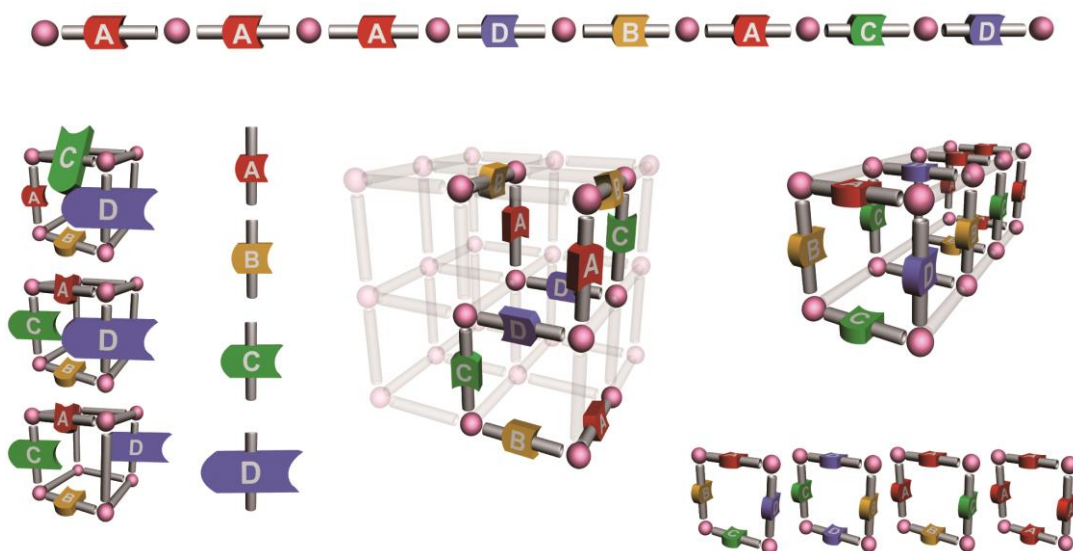


Figure 1. 8. Schematic representation of the concept of multivariate MOFs (MTV-MOFs) using a variety of organic linkers.

### 3. Synthesis Routes of MOFs

Numerous ways regarding the synthesis of MOFs were reported[29]. However, the most common route is the solvothermal method (liquid phase), in which separate solutions of the metal salt and the organic linker are prepared and then, mixed together in a reaction container that is held at high temperature[30]. Alternative to the

solvothermal method, researchers attempted easier ways such as the solid state synthesis where the organic linker is mixed with the metal salt without the incorporation of any solvent[31]. In addition to these traditional synthesis methods, other efficient advanced methods are being utilized including the microwave assisted synthesis[32] and the sonochemical synthesis[33].

#### a. Solvothermal Synthesis

The energy required in this route of synthesis is the thermal energy. The metal salt and the organic linker are placed in a vial, mixed and dissolved in a suitable solvent or a mixture of solvents to overcome the solubility issues[34]. The organic solvents that are considered friendly to MOFs and are mostly used in their synthesis are N, N-Dimethyl formamide (DMF), N, N-Diethyl formamide (DEF), dichloromethane, ethanol, methanol, and acetonitrile[12, 35, 36]. The reaction mixture is carried at high temperatures. For temperatures lower than the boiling point of the solvent, the glass scintillation vials are commonly used, however for higher temperatures, teflon autoclave reactors are utilized[37]. The advantage of this method over other conventional methods resides in achieving crystal morphologies down to the nanoscale[38].

#### b. Mechanochemical Synthesis

In the mechanochemical synthesis, the intramolecular bonds are broken by applying mechanical forces and then a chemical reaction occurs in a solvent-free medium[39]. The first MOF using mechanochemical synthesis was reported in 2006, and it was obtained by effectively grinding copper acetate and isonicotinic acid



together[40]. When using this synthesis method, the metal salts could be replaced by metal oxides which lead to the formation of only water as a side product[41]. In addition to that, the reactions could be achieved at room temperature without using solvents especially organic solvents that may present harmful concerns on the environment. Nonetheless, the short time reaction in the mechanochemical synthesis is considered an important point as in this range of time, quantifiable yields of small sized particles could be produced[42]. The main struggle of using this method relies in the difficulty of controlling the mechanism of the proceeding reaction. However, Tomislav Friscic et al. managed to solve this issue through in situ diffraction of synchrotron X-rays with high energies[43].

#### c. Slow-Evaporation Synthesis

Similar to the solvothermal synthesis, the slow evaporation method is a conventional way where the metal salt and the organic ligand are mixed in a vial using the appropriate solvents. In this method, the system is carried at a constant temperature, usually room temperature and the solvents evaporate leaving behind the product which is the MOF in this case[44]. This method is preferred because it is pertinent at room temperature, however; the product takes more time to be formed as compared to other conventional methods. To overcome this drawback, a mixture of solvents having a low boiling point is used and thereby, increasing the solubility of the involved reagents.

#### d. Microwave Assisted Synthesis

It is considered an efficient innovative method for the synthesis of MOFs[45]. It relies on the interaction of the electromagnetic waves with the portable electric

charges. These electric charges are represented as electrons/ions in the solid materials and as solvent molecules/ions in solutions[46]. As compared to other synthesis techniques, in the microwave assisted solvothermal synthesis, one could control the nucleation of the MOF particles in the solution[47] and monitor certain reaction variables such as the temperature and the pressure[48]. In addition to that, the synthesis process could be attained in a diminutive duration [47].

e. Electrochemical Synthesis

Unlike other synthesis routes, the electrochemical synthesis utilizes only the metal ions and eliminates the anions as the chlorides, nitrates, and sulfates which pose hazardous concerns when produced in large scale[49, 50]. In this technique, the organic linker is dissolved in the presence of an electrolyte or a conducting salt and then the metal ions are constantly added to the reaction medium via anodic dissolution[51]. Protic solvents are used to suppress the deposition of the metal on the cathode, however, this will result in the formation of H<sub>2</sub>, so in this case it is preferred to substitute the protic solvents by other compounds as acrylic esters that could be easily reduced[46, 52]. The main advantages of exploiting this synthesis method as compared to other methods, is that the MOFs are produced in vast industrial scales under relatively mild circumstances and in a short period[53].

f. Sonochemical Synthesis

Sonochemical synthesis is based on applying excessive ultrasonic radiation of high energy and thereby, inducing a chemical change in the reagent molecules[54, 55]. It is important to know that the ultrasonic radiation falls in the range between 20 kHz

and 10 MHz and so, it has a higher wavelength than the dimensions of the molecules meaning that the chemical reactions are induced by a certain process rather than the ultrasound-molecules interaction[56]. This process is known by the cavitation process, in which the liquid interacts with the high energy ultrasound, thus forming high and low pressure areas in the liquid[57]. In the low pressure area, bubbles or as known by cavities are formed as a result of the difference between the pressure of this area being lower than that of the vapor pressure of the solvent. After that, these bubbles tend to grow via the dissemination of the volume of the solute into the bubble volume, this will thereby lead to the buildup of the ultrasonic energy and the bubbles will continue to increase in size until the extreme is reached, where their stability will get lost and directly collapse. Then, spots with high temperatures and pressures known as the hot spots are formed from the bursting bubbles, and these spots are responsible for the creation of excess crystallization nuclei[58-60]. Sonochemical method aims for synthesizing MOFs rapidly at room temperature in a fast and environmentally friendly medium[61].

#### ***4. Applications of MOFs***

One of the most interesting features of MOFs is that every component of their structure can be varied and functionalized to optimize gas sorption/selectivity[62, 63]. This can be achieved by functionalizing the MOF structures either by the substitution or modification of the organic ligands and/or the metal centers. Their pores are homogenous in size and coherent in their function, an aspect that leads to non-hysteretic recyclability of uptake and release of gases. Moreover, the molecular structure of these framework materials shows that, unlike other porous media, the ‘pores in MOFs have no walls’, which leads to facile uptake and release of carbon dioxide (several orders of

magnitude faster than in zeolites and porous carbon materials)[64]. Finally, MOFs have thermal stability in air up to 400 °C and high chemical stability (aqueous and organic solvents). These unique properties open the door to countless applications in gas adsorption or separation, catalysis, and sensing[65]. Recently, it was demonstrated that the properties of MOFs could be closely related to its size and morphology. Indeed, control over the degree of size and shape is achievable through the chemical reaction route as well as the crystal nucleation and growth rates during synthesis. More interestingly, when MOFs crystals are downsized to nanometer scale, the crystal interfaces are anticipated to influence the sorption kinetics or even the sorption type[62-64, 66]. Moreover, in the porous MOFs nanocrystals, the diffusion length is decreased, which is very important in catalysis and sorption in liquid phase. Indeed, it was shown that miniaturizing and controlling the crystal size and morphology of the porous MOFs used as porous membranes, thin film or carrier particles for drug delivery are of utmost importance in the enhancement of the performance of these materials[62]. In the next section we will describe briefly some of the most interesting applications of MOFs in gas storage, catalysis, sensing and drug delivery[67-70].

#### a. MOFs as catalysts

In addition to the storage and separation properties, MOFs have enormous potential in catalysis due to their unique structures and properties[71]. The presence of the organic part in MOFs lead to a lighter weight material, in addition to the diversity in the diversity and the tuneability in the size of the pores leading to an enhancement in the selectivity and the affinity towards the target materials, make from MOFs impending candidates for catalysis[72]. Furthermore, MOFs provide a high density of available

active sites. In most of the catalytic applications, either the metal moiety or the organic linker molecules is involved. Nonetheless, the regioselectivity or shape- or size-selectivity could be induced by the arrangement of the open metal centers in the pore channels a regular form and this promising tool could be simply offered by MOFs[73, 74]. After the catalytic studies on phosphonates[75], catalysis by MOFs includes now cyanosilylation, the Diels–Alder reaction, the hydrogenation, esterification, CO oxidation, and many others[76-78].

#### b. Gas Storage

Gases such as H<sub>2</sub>, CH<sub>4</sub> and many others are considered vital sources for the energy production. However, storing such gases require special high pressure tanks that are exceedingly expensive[79]. Alternative to these costly tanks, recently MOFs which have high surface areas and tunable pore size, have been introduced as cheaper and practical candidates[80].

Hydrogen gas is known by its high gravimetric heat of combustion and thereby, is considered a suitable contestant for energy production. However, storing the hydrogen gas at ambient pressures and temperatures is challenging because of its low density, therefore, this suppresses the usage of this gas as an effective source of fuel[81]. Lately, MOFs have outperformed this problem by having high surface areas, sparse weight, and open metal sites that facilitate the interaction with the hydrogen gas resulting in a higher H<sub>2</sub> uptake[82, 83]. Examples of MOFs which are well known for their effective H<sub>2</sub> gas storage are MOF-177[84], MOF-199, MOF-5, and many others[85].

As a result of the rapid development in the industrial field, CO<sub>2</sub> emissions from raw material as coal and natural gas are rising continuously and have reached levels that possess a real threat on the living beings. In order to minimize the CO<sub>2</sub> emissions, MOFs functionalized with polar substituents at their pores have succeeded as efficient adsorbents and recorded high CO<sub>2</sub> uptakes[86, 87]. NU-110E which has the highest reported surface area till now (7140 m<sup>2</sup>/g) has recorded the largest CO<sub>2</sub> uptake (2400 m<sup>2</sup>/g)[88, 89].

CH<sub>4</sub> gas is considered a dynamic fuel due to its decent gravimetric heat of combustion and it constitutes 95% of the natural gas. Similar to the H<sub>2</sub> and CO<sub>2</sub> gas storage, the high methane uptake presented by MOFs relies mainly on the open metal centers that facilitate and enhance the interactions with the methane gas[90]. In addition to that, doping MOFs with metal ions would further boost the uptake efficiency, for instance, lithium doped MOF-199 exhibits an enhanced CH<sub>4</sub> by about 200% as compared to the unmodified one[91].

### c. MOFs as sensors

MOFs offer wide opportunities in the realms of luminescence and sensing. Scientists are interested in these materials as sensors because of their hybrid structure (metal ions connected with organic linkers). In addition to that, MOFs in their high crystalline form have well-defined predictable structure that serves as an incubator environment to the chromophores[92, 93]. The most used metal ions in luminescence are the lanthanide metal ions because of the transitions of the electrons from the d shells to their corresponding higher energy f shells along with the photon emission. These lanthanide metal ions coordinate with highly adsorbing ligands, thus improving the

luminescent properties of the MOFs[94]. It should be noted that when using transition-metals, the luminescent properties come only from the organic linkers, whereby in this case, the most commonly witnessed electronic transitions are the  $\pi$ - $\pi^*$  and the  $n$ - $\pi^*$ [95]. The most commonly known ligands for their luminescent properties are those having extended  $\pi$ -systems with substantial conjugation such as naphthalene, anthracene and pyrene[96].

#### d. MOFs in drug delivery

Conventional drug storage and delivery systems are mainly either organic or inorganic systems. Such pure systems may have some drawbacks, as for the organic systems; the mechanism of releasing the drug is not controlled, although the biocompatibility extent is very high. On the other hand, inorganic delivering systems have ordered porous structures and thereby the rate at which the adsorbed drugs are delivered could be controlled. However, such inorganic linkers suffer from a low loading capacity[97]. Recently, the usage of MOFs as drug storage and delivery materials has become an imperative area of research owing to their hybrid nature that consists of both the organic and the inorganic materials[98-100]. However, it should be taken into consideration that MOFs with a small pore size is not efficient as this restricts the number of the drug molecules destined in the framework. Therefore, for such application, it is better to utilize mesoporous MOFs such as the MIL-100 and MIL-101 having pore diameters of around 29 Å and 34 Å, respectively[101]. Nonetheless, MOFs at the nanoscale (NMOFs) characterized by a virtuous biodegradability along with a trivial cytotoxicity have proven to be ideal candidates for numerous applications in the realm of nanomedicine. In this context, the collaborative research work of Bo Wang and

Ying-Wei Yang resulted in the synthesis of a nanosized MOF made from dicarboxylate moieties coordinated with zinc ions. After that, the external surface of the MOF was coated with pyridinium moieties that are charged through loading it with either an anticancer drug such as doxorubicin hydrochloride and further capped with the negatively charged pillarenes macrocycles. When the MOF is exposed to the acidic medium present in the tumor cells, the anionic pillarenes will be protonated, thereby leading to their alienation from the framework and the release of the drug in its active form directly to the target medium[102, 103].

e. Water Purification

Water contaminated with heavy metals arising from various industrial applications is considered a major threat for the ecosystem. The presence of heavy metals in the aquatic medium such as cadmium, lead and mercury may possess toxic side effects even at very low concentrations[104]. For this reason, it is important to develop novel systems and materials that are able to remove such toxic pollutants efficiently and cost-effectively. In this context, MOFs are considered good candidates for eliminating such heavy metals via adsorption into its pores[105]. For instance, Wang et al. designed a  $\text{Cu}_3(\text{BTC})_2$  MOF functionalized with sulfonic acid groups at the pore surface which displayed a tendency and selectivity for adsorbing the cadmium ions from aqueous solution[106]. Other major pollutants that resolve in water are dye molecules, which are colored organic materials that tend to bind to specific substrates. It could be either naturally occurring or synthetic most of which released from countless industries including, textile manufacturing, cosmetics, medicine, food coloring and many others. Such dyes present a high stability in aqueous solutions owing to their



chemical structure, which coarsens their elimination from the industrial sewage water that could subsequently exonerate into the water bulk and threatens the humans and aquatic life. For this reason, several methods have been extensively engaged in the treatment and removal of dyes from adulterated water. Such techniques are essentially classified into three categories: Biological method including aerobic and anaerobic treatments[107], physical such as adsorption and membrane filtration processes whereas chemical processes include eliminating these dyes via oxidizing agents such as hydrogen peroxide and ozone or inducing their precipitation by using alkaline material. However, it has been demonstrated that among the proposed methods, adsorption is considered the most efficacious method due to its high feasibility and low cost[108]. In the adsorption process, a solid body (adsorbent) tends to attract a specific solute in the solution (adsorbate), to its surface via forces of attraction. In this context, MOFs served as good candidates for the adsorption of various dyes, although there are only few reported MOFs in this field and their study is still in the infancy stage[109]. An important example is the iron terephthalate MOF-235, used for the adsorption of dyes with different charges including the anionic dye Methyl Orange and the cationic Methylene Blue with adsorption capacities that further surpassed those of the typical activated carbon[110].

## **B. Reaction-Diffusion Framework (RDF)**

### ***1. RDF in Nature***

RDF appears to have a significant impact on different animate and inanimate systems in nature having different scales and miscellaneous properties. For the living species, convoluted RD processes are involved mainly for regulatory and gesturing

processes. For instance, abundant regulatory mechanisms occurring in cells owe to the calcium signals arbitrated by chemical waves, which in turn are formed due to complex RD progressions. On the other hand, motionless systems make use of RD in a simpler manner than that of living systems through employing inorganic materials in order to form spatially extended structures. These inorganic chemicals already existing in nature tend to react and form intermittent layers comprised from diverse natures of precipitates. A fascinating example is the iris agates (Fig. 1.9 e), which reveals interchanging layers of the high defective chalcedony and the low defect quartz formed by the deposition of two different types of minerals. In addition to the cave stalactites (Fig. 1.9 h), that acquire their textures through certain RD progressions. The majority of such systems owing their shapes to RD progresses exist in large scales, and studying such systems could be helpful for establishing our unique RD microsystems in the lab[111].

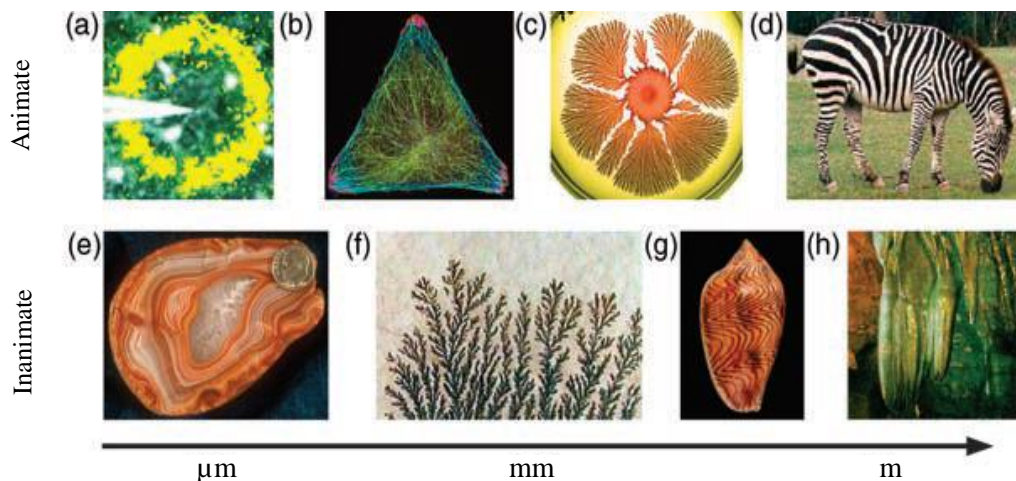


Figure 1. 9. Illustrations of diverse animate (a-d) and inanimate (e-h) RDF systems on different length scales ( $\mu\text{m}$ , mm, m). Reprinted with permission from ref. [112]. Copyright 2009 John Wiley & Sons.

## 2. RDF in Chemistry

Reaction-Diffusion systems aim on synthesizing solid material far from equilibrium through locally transmuting the involved components into each other by chemical reactions and transporting them in space via diffusion. The prominence of this method relies on studying and controlling the size of the particles obtained within bands under mild conditions[112]. Such an example is the synthesis of lanthanum hydroxide and the control of its size and morphology through varying certain parameters including the temperature, concentration of the gel matrix, and the concentration of the corresponding electrolytes[113]. Another beneficial application of RDF is the ability to attain a sensible mechanism for the polymorphic transition of  $\alpha$ -Co(OH)<sub>2</sub> into  $\beta$ -Co(OH)<sub>2</sub>[114].

### a. Diffusion

Diffusion is a non-equilibrium procedure, though it results in an equilibrium state by the transfer or the movement of matter from a high concentration region to a low concentration region. Thereby fundamentally, diffusion is compelled by the concentration gradient of the material[115]. Adolf Fick first described diffusion in the nineteenth century via Fick's first law which states that the flux is proportional to the negative value of the concentration gradient of the substance (Equation 1.1),

$$J_O(x, t) = - D_0 \frac{\partial C_O(x, t)}{\partial x} \quad (1.1)$$

where  $D$  is the diffusion coefficient,  $J_o$  is the diffusion flux of the substance  $O$ ,  $C_o$  is the concentration of the substance  $O$  and  $x$  is the distance taken by the species  $O$  to approach the reaction region at a certain time  $t$ [116]. It is clear from Fick's first law that the mass transfer gets larger as the concentration gradient becomes steeper.

Diffusion has three main pathways which they are bulk, grain-boundary, and surface diffusion. As for the grain boundary diffusion, it occurs in polycrystalline solid particles that are concentrated on the boundaries of the grains due to the misalignments in the crystals orientations[117], whereas the surface diffusion involves the movement of the particles which could be atoms or molecules found on the solid material surface.[118]. Conversely, in bulk diffusion also known as the lattice diffusion, the atoms diffuse within the lattice of the crystal[119]. Due to the higher concentration of the defects on the surface, surface diffusion occurs much faster than the grain boundary diffusion, which in turn is faster than that of the bulk[120]. Within our work, diffusion occurs in a gel matrix containing organic ligands. Upon the addition of a liquid solution containing metal ions, a precipitate is formed, which is the MOF. Thereby, the formation of the MOF is controlled by the bulk diffusion.

Moreover, there are several factors that affect the rate of diffusion, such as the temperature. As the temperature increases, the particles will move faster thereby speeding up the diffusion and vice versa[121]. In addition to that, the diffusion rate increases as the concentration gradient increases. Nonetheless, the nature of the diffusing species, size and its crystal structure all have a realizable effect on the rate of diffusion.

#### b. Nucleation and Supersaturation

Nucleation is the foremost stage of producing new crystalline material from a solution. It transpires as the atoms, ions, or the molecules making up the reactants are repositioned to generate the products in the form of clusters known as nuclei, big enough to grow and proceed in an irreversible manner to the macroscopic size[122]. Nucleation could be classified into two main categories, homogeneous and heterogeneous nucleation[123]. In the former, nucleation occurs within the particles of the old phase,[124] whereas in the latter, nucleation occurs on alien surfaces such as dust particles or impurities[125].

For the crystallization to occur, the solution should be supersaturated. Thereby, supersaturation is considered the driving potency for the nucleation of the crystal and its subsequent growth. Supersaturation ensues when the solvent contains dissolved solute in excess or above the limit that the liquid could accommodate. In other words, it is the chemical potential difference between the molecule found in the solution and that of the molecule found in the crystal's bulk[126]. This is explained by the following equation:

$$\Delta\mu = \mu_s - \mu_B \quad (1.2)$$

Where  $\mu_s$  is the chemical potential of the molecule in the solution and  $\mu_B$  is the chemical potential of the molecule in the bulk. It is found that when  $\Delta\mu > 0$  supersaturation of the solution befalls, whereas when  $\Delta\mu < 0$  dissolution occurs and the nucleus will dissolve[127].

### c. Crystal Growth

Crystal growth is a paramount stage in the crystal formation process. Following a successful nucleation process, crystal growth tends to be more auspicious were an increase in the crystal size occurs due to an atom or molecule integrated on its surface. It is worth mentioning that the crystal growth stage together with the nucleation process aim to dictate the ultimate particle size dispersion. Moreover, being able to control the circumstances and the rate of the growth mechanism is important to produce highly pure crystals[128].

### **C. Objectives**

As previously stated, MOFs are a new class of highly porous crystalline materials. They are built from metal clusters joined by organic ligands via strong coordination bonds. The hybrid nature of these materials granted them superior features and properties that preceded vigorously other materials having a pure organic or inorganic nature. Therefore, scientists all over the World harnessed their efforts to upsurge their research in the field of MOFs and optimize the properties of these materials in order to reach the ultimate efficiency when integrated into diverse applications. For instance, MOF-199 also known by HKUST-1 with the formula,  $[\text{Cu}_3 (\text{BTC})_2 (\text{H}_2\text{O})_3]_n$  is considered one of the most studied and furthestmost prominent MOFs. The eminence of this MOF is due to its distinctive features such as the high surface area ranging between 1100 and 2200  $\text{m}^2/\text{g}$ , ease of preparation using different synthesis methods, low density, thermal stability under temperatures reaching 350 °C and chemical stability in water. All of these distinguishing characteristics made from

MOF-199 a suitable candidate for numerous applications such as H<sub>2</sub> and CO<sub>2</sub> storage, catalysis, drug storage and delivery.

It is evident that the characteristics and the properties of MOF-199 strongly depend on the synthesis route, temperature of the reaction, proportions of the metal ions and the organic linkers with respect to each other, in addition to the nature and the extent of the solvents utilized. The objective of this work is to synthesize for the first time MOF-199 single crystals using the RDF method at room temperature. Different experimental conditions such as the temperature of the medium, concentration of the inner and the agar gel, the type of the gel and the metal source in the outer were varied and their effect on the crystal size, morphology, stability, porosity and many other properties were investigated.

In the second part of this thesis, we exploited the success of the synthesis of MOF-199 using RDF system and introduced heterogeneity into it by incorporating an additional linker 5-Hydroxyisophthalic acid to the inner part. It is noteworthy to mention that when the organic linker 5-Hydroxyisophthalic acid was used alone in the RDF system, no precipitate was formed. This approach is demanding and can be confronted by either the disorder in the crystal structure or the lack of a single homogenous phase (mixture of linkers). Similar to MOF-199, MTV-MOFs were subjected to various characterization techniques. In this occasion, we approved the homogeneity of the MTV- MOF (OH-BDC:BTC) by comparing the PXRD patterns with respect to MOF-199. Furthermore, we examined the degree of incorporation of the linkers within the framework via <sup>1</sup>H-NMR technique. In addition, the morphology, thermal stability and surface area of the MTV-MOF (OH-BDC:BTC) with different proportions of the linkers was investigated via SEM, TGA and BET respectively. The

advantages from introducing heterogeneity within the MOF structure are countless especially on the application level. In this regard, we tested the adsorptive activity of the produced MOF systems via RDF method (MOF-199 and MTV MOFs) on Methylene Blue dye (MB) and compared their performance.



## CHAPTER II

# MOF-199 SINGLE CRYSTALS VIA REACTION-DIFFUSION FRAMEWORK: SYNTHESIS PROCEDURE AND CHARACTERIZATION

### A. Materials and Methods

#### 1. Materials

$\text{Cu}(\text{OAc})_2 \cdot \text{H}_2\text{O}$  and 1,3,5-Benzenetricarboxylic acid (BTC) were purchased from Acros Organics, the agar gel from Bacto, copper nitrate trihydrate  $\text{Cu}(\text{NO}_3)_2 \cdot 3\text{H}_2\text{O}$ , N-N-Dimethyl Formamide (DMF), Dichloromethane (DCM) and Ethanol absolute from Sigma Aldrich, Dibenzylidene sorbitol (DBS) from HENAN SUNLAKE ENTERPRISE, LB Lennox agar gel from Conda. The following reagents were used as received without any further purification.

#### 2. Preparation of MOF-199 Single Crystals

Our system is based on the diffusion of the metal salt through the gel matrix where the organic linker is immobilized. Regarding the preparation of MOF-199, the inner part consists of the ligand BTC (10 mM) mixed with agar gel in an Ethanol/Water (50%/50%) solution. The whole mixture is then heated up to a convenient temperature so that the agar gel becomes clear and directly transferred into a Pyrex test tube filling its two thirds, which is then covered and left until the agar has congealed completely. When the gel has solidified completely, the outer portion which consists of the metal salt  $\text{Cu}(\text{OAc})_2 \cdot \text{H}_2\text{O}$  (100 mM) dissolved in an Ethanol/Water (10%/90%) mixture is added, filling the remaining volume of the tube. Finally, the tube is covered and left for

the reaction-diffusion process. It should be noted that the concentration of the outer have to be 10 times higher than that of the inner to allow the diffusion process, Fig. 2.1 (A). The formed MOF-199 precipitate is extracted by heating the agar gel in double distilled water with continuous stirring until the gel becomes clear. Then, the washed precipitate is collected and separated from the supernatant solution through centrifugation. After that, the obtained MOF-199 particles are washed with DMF over 3 days and then with DCM by solvent exchange. Finally, the sample is subjected to vacuum drying for 10 hours so that it becomes dry and ready to be characterized with the corresponding techniques, Fig. 2.1 (B).

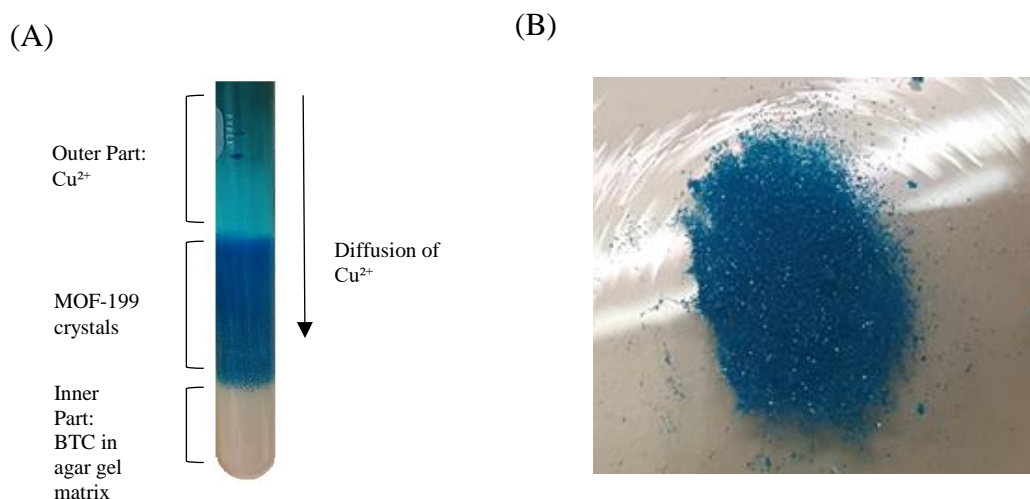


Figure 2. 1. (A) Schematic representation of the MOF-199 synthesis via RDF. (B) MOF-199 crystals formed after washing and drying.

## B. Characterization of MOF-199 Single Crystals

MOF-199 crystals obtained are collected, washed and characterized via several techniques including PXRD, SEM, TGA and BET.

### ***1. Powder X-ray Diffraction (PXRD)***

PXRD is considered a fingerprint for the examined sample, as the PXRD pattern is unique for each sample. PXRD is a non-destructive analytical technique through which the chemical composition, structure, and many other physical characteristics could be determined. Throughout our work, X-ray diffraction (XRD) measurements were conducted on the XRD D8 Advance X-ray diffractometer using the Cu-K $\alpha$  radiation ( $\lambda = 1.5406 \text{ \AA}$ ) at 40kV and 40 mA. PXRD can be used to determine the size of the particle in accordance to Scherrer equation:

$$\tau = K \lambda / \beta \cos \theta \quad (2.1)$$

where  $\tau$  is the average crystallite size,  $K$  is Scherrer constant,  $\lambda$  is the wavelength of the X-ray,  $\beta$  is the line broadening at the full width of the half maximum (FWHM).

### ***2. Scanning Electron Microscopy Analysis (SEM)***

In SEM, the sample is subjected to scanning with a beam of electrons that interacts with the atoms of the sample generating thereby signals that could be transformed into beneficial information which is in this case the image. MOF-199 crystals were dispersed in a dichloromethane and few droplets were deposited on carbon coated stubs, dried at room temperature, and plated with gold. SEM images were conducted on the FEI Quanta 600 FEG-SEM instrument.

### ***3. Nitrogen Adsorption and BET Calculation***

Nitrogen isotherms are used to analyze the surface area and the pore volume of the porous samples. In this thesis, the sample (MOF-199) was degassed at 80 °C under vacuum for 10 h prior to the sorption analysis measurements. The BET surface area and

the pore volume of the samples were calculated by the surface area analyzer (NOVA 2200e).

#### ***4. Thermal Gravimetric Analysis***

The TGA relates the changes in weight of the sample with the temperature and thus, determines the thermal stability of the given sample in an adjusted atmosphere. Thermogravimetric analysis (TGA) were obtained at a ramp rate of 5 °C/min from 30 °C to 1000 °C under nitrogen atmosphere on NETZSCH TG 209F1 Libra TGA209F1D-0152-L.

### **C. Results and Discussion**

In the following section we discussed the results obtained from the different techniques mentioned in section B and compare these results to the MOF-199 synthesized using other routes reported in literature. Furthermore, we examined the influence and control of varying different experimental parameters including the temperature, concentrations of the inner and the gel on the size and the morphology of the obtained MOF-199 crystals. Finally, we conducted a kinetic study to investigate the rate of diffusion and capture the possible transition in the structure of the MOF-199 crystals.

#### ***1. Powder X-ray diffraction (PXRD) patterns of the obtained MOF-199 by RDF***

The PXRD pattern of the obtained crystals was recorded and compared to the simulated pattern. It is clear from Fig. 2.2 (B), that the PXRD patterns of the MOF-199 crystals synthesized by RDF have sharp narrow peaks, which perfectly match the

characteristic peaks corresponding to the theoretical ones thereby, revealing the high crystallinity and purity of the synthesized sample. The PXRD was indexed in a cubic structure of MOF-199 with a lattice parameter value of  $a= 26.30 \text{ \AA}$ .

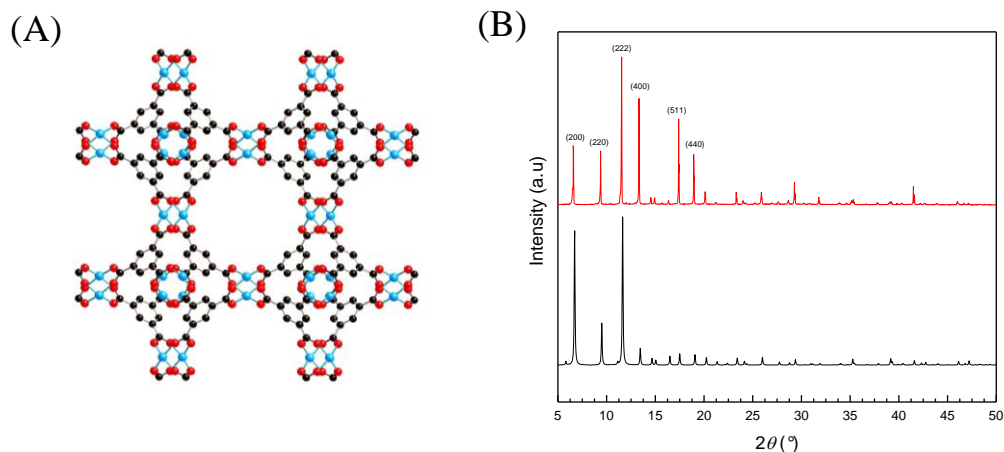


Figure 2. (A) Crystal structure of MOF-199. C, black; O, red; Cu, blue. Hydrogen atoms are removed for clarity. (B) PXRD patterns of MOF-199 crystals of (a) calculated one compared to (b) MOF-199 prepared via RDF.

## 2. Determining the morphology of the MOF-199 single crystals

The microscopic image in Fig. 2.3 shows that the MOF-199 crystals produced by the RDF method have a cubic morphology. Further investigation on the morphology of the crystals was done using SEM (Fig. 2.4), which also confirms the highly pure cubic morphology of the MOF-199 single crystals with the absence of any impurities.

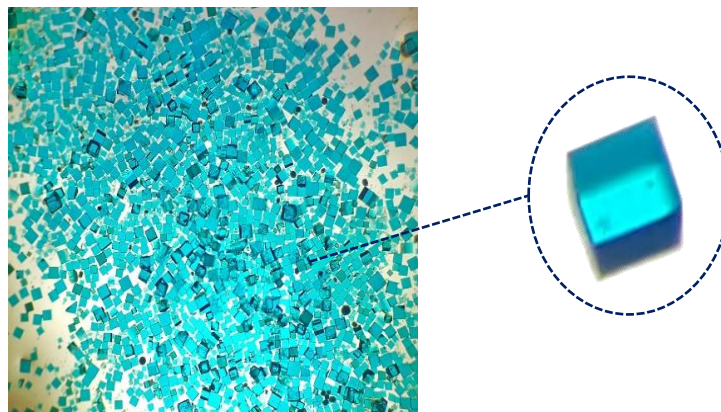


Figure 2. 3. Optical microscope images showing the cubic morphology of the MOF-199 prepared by RDF method.

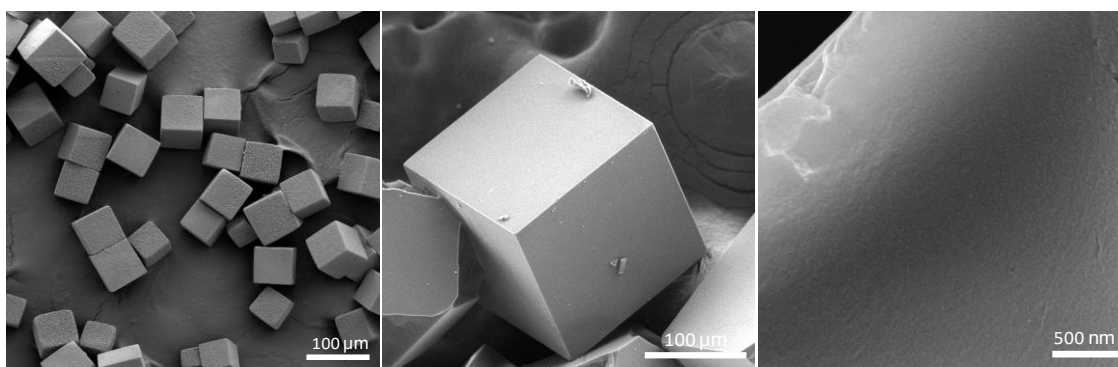


Figure 2. 4. SEM images of MOF-199 taken at different scales.

### ***3. The surface area of MOF-199 synthesized via RDF***

The surface area of the obtained MOF-199 is calculated to be  $1236 \text{ m}^2/\text{g}$  with a pore volume value of  $0.56 \text{ cc/g}$  and a pore radius  $12.2 \text{ \AA}$ . All these values are in agreement with the reported one in the literature. It is clear from the  $\text{N}_2$  isotherm shown in Fig. 2.5, that MOF-199 sample exhibits Type I isotherm. The long straight horizontal plateau indicates that it is limited to the completion of the single monolayer of the adsorbate ( $\text{N}_2$  gas), on the surface of the adsorbent, which is MOF-199, thereby signifying the microporous nature of MOF-199. This result is congruent with the SEM

images in Fig. 2.4 that shows a smooth surface of the obtained MOF-199 crystals, in addition to the peaks appearing at low  $2\theta$  angles in the XRD pattern.

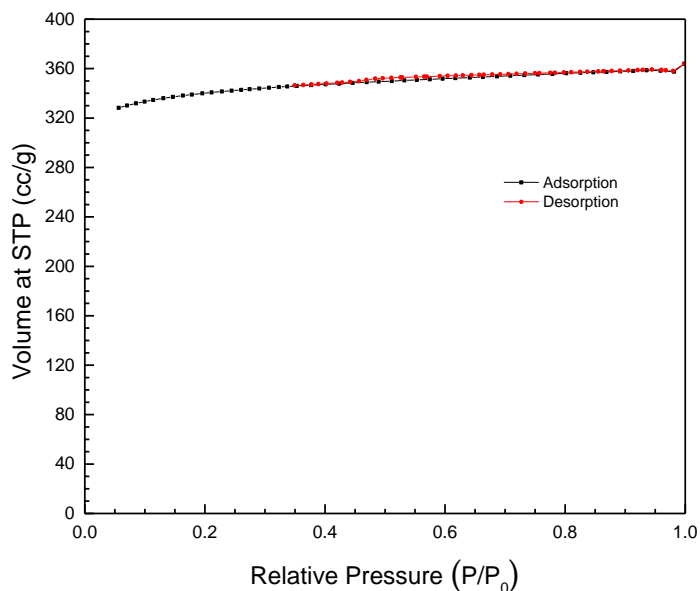


Figure 2. 5. Nitrogen physisorption isotherm of MOF-199 synthesized via RDF.

#### ***4. Thermal Stability of the obtained MOF-199***

MOF-199 exhibits a high thermal stability up to 350 °C. The TGA curve plot in Fig. 2.6 shows the as synthesized MOF-199 were the sample is directly analyzed without prior washing with DMF and the activated MOF-199 were the sample is washed several times with DMF followed by solvent exchange with DCM and the pores are evacuated by vacuum drying for about 12 hours. Fig. 2.6 shows two major weight losses for MOF-199 which is similar to the reported ones in literature. The first was at around 100 °C with only 5% loss suggesting the evaporation or the volatilization of the solvent used for washing the sample prior to analysis. The second was at around 350 °C with 58% mass loss indicating the thermal decomposition of the MOF-199 framework. The residual weight remaining after the decomposition could coincide to the formation

of copper oxide, the remaining carbon or metallic copper. It should be noted that all the samples throughout this thesis used in TGA analysis are activated.

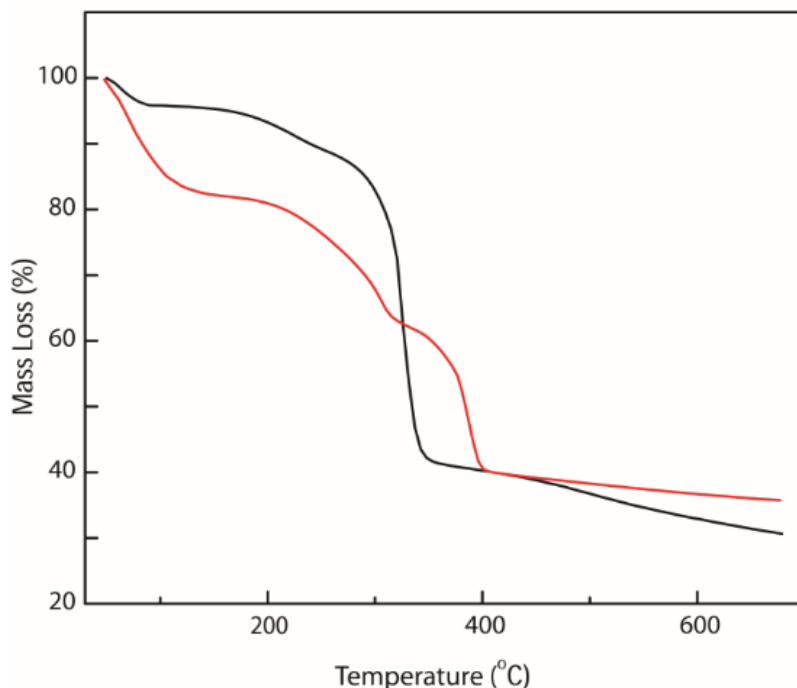


Figure 2. 6. Thermogravimetric curves of MOF-199 under nitrogen atmosphere with a heating rate of  $3^{\circ}\text{C}\cdot\text{min}^{-1}$  and a temperature ranging from  $30^{\circ}\text{C}$  to  $700^{\circ}\text{C}$  of the as synthesized MOF-199 (red), activated MOF-199 (black).

### **5. Yield of MOF-199 synthesized by RDF**

One of the major problems of MOF-199 synthesis is to scale it up. In our procedure, MOF-199 was prepared at different scales 100, 250, 500, and 1000 mL (Fig. 2.7). By scaling up, neither the quality nor the morphology of the crystal has been altered. Gigantic amounts of the MOF (up to 10 g) were produced at the large scales (500 and 1000 mL) and the yield reached 90%. This shows a possibility to synthesize large amounts of this MOF in a relatively short period of time using this



environmentally friendly and profitable method which makes it really interesting on the industrial level.



Figure 2. 7. MOF-199 prepared via RDF process at different scales

### ***6. Size and morphology control of MOF-199 single crystals***

It has been demonstrated that the size and morphology of the MOF crystals play a key role in many applications. Different experimental conditions for the synthesis of MOF-199 single crystals were varied in order to investigate their effect on the size and the morphology of the crystals. Such parameters include: The concentration of BTC (inner), agar gel concentration, temperature, copper source in the outer, type of gel and reversing the components of the inner and the outer ( BTC in the outer and  $\text{Cu}(\text{OAc})_2 \cdot \text{H}_2\text{O}$  in the inner).

#### **a. Effect of temperature**

MOF-199 was prepared in a set of five tubes, each was subjected to a specific temperature ( $7^\circ\text{C}$ ,  $15^\circ\text{C}$ ,  $20^\circ\text{C}$ ,  $25^\circ\text{C}$ , and  $30^\circ\text{C}$ ). After that, the formed precipitate was divided into consecutive bands each 0.5 cm. The histogram and the graph in Fig. 2.8 (A)

and (B) respectively reveal that as the temperature increases from 7°C to 30°C, the rate of the diffusion increases and this is evident from the number of bands which increased from three (at 7 °C) to six bands (at 30 °C) respectively. This refers back to the kinetics of the MOF formation, which rises with temperature, thereby yielding a faster and more uniform diffusion. Obviously, at high temperatures the rate of diffusion went faster so the number of bands will be more within the same time interval and the size of the crystals in the final band will be much greater (e.g the maximum average particle size is 162 μm at 30 °C) as compared to those in the final band of the tubes at low temperatures (e.g the maximum average particle size is 40 μm at 7 °C). The importance of this study relies in adjusting and controlling the size of the MOF crystals in accordance to a specific targeted application, thus if the application needed small sized crystals, the experiment could be performed at low temperatures and vice versa.

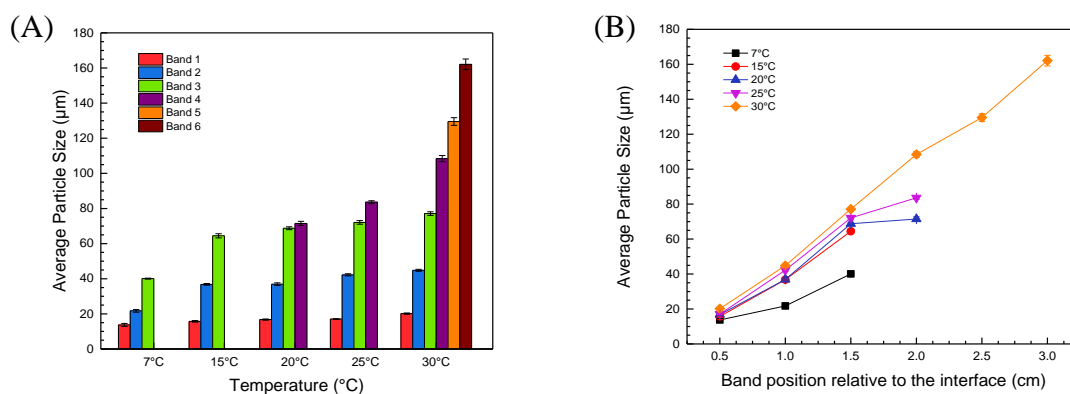


Figure 2. 8. (A) Histogram showing the variation of the average particle size of MOF-199 (μm) as a function of temperature (°C). (B) Plot showing the average particle size (μm) in each band at different temperatures.

The SEM images corresponding to the bands in each tube at different temperatures are represented in Fig. 2.9. The increase in the number of bands at higher

temperatures within the same period is evident however; the cubic morphology of the MOF-199 crystals was not altered.

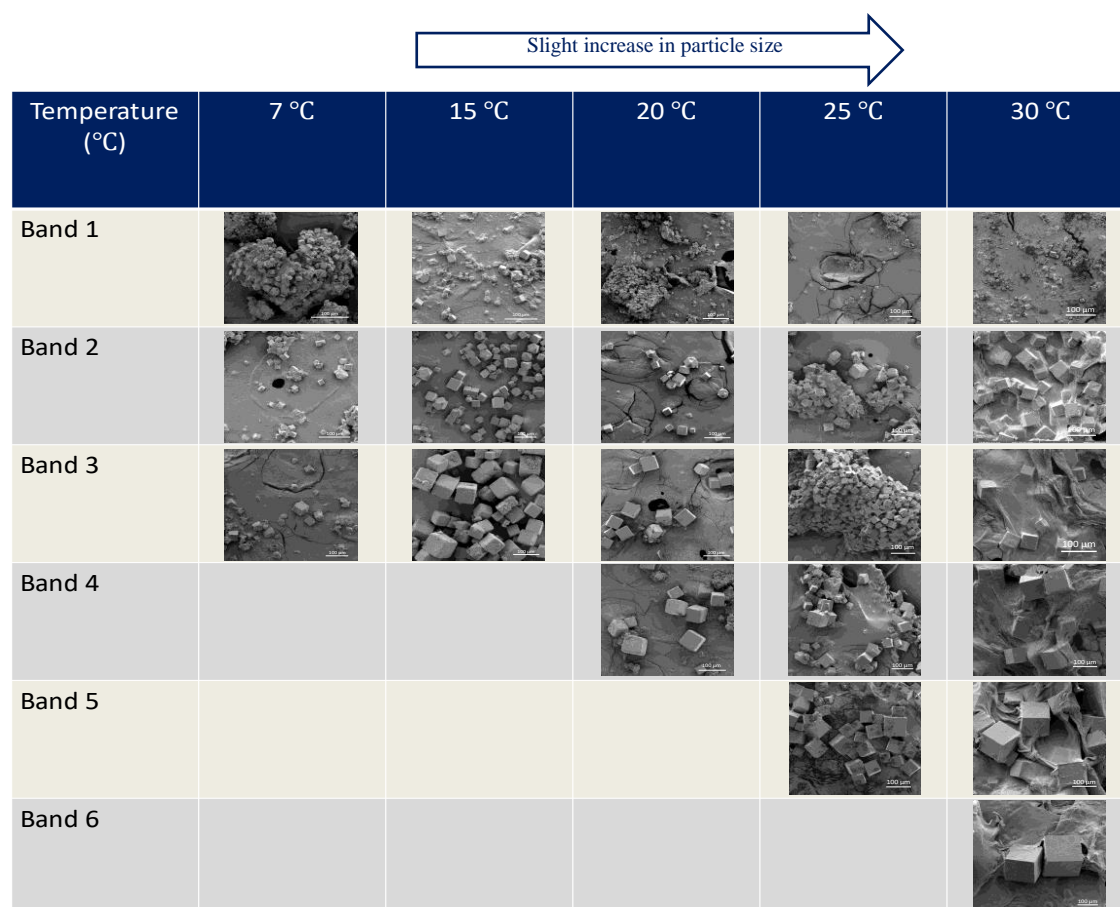


Figure 2. 9. SEM images showing the growth pattern of the MOF-199 particles at different temperatures and same inner concentration (10mM) in consecutive regions of the tube (0.5cm each). Scale bar 100  $\mu$ m.

#### b. Inner Concentration [BTC]

In order to study the effect of the linker concentration, MOF-199 crystals were prepared using seven different inner concentrations [BTC] (0.05 mM, 1 mM, 3 mM, 5 mM, 10 mM, 20 mM and 50 mM) at room temperature in 1% agar gel and SEM images of the different samples were collected.

By looking at the graphs in Fig. 2.10 (A) and (B), it is evident that the average particle size of the obtained MOF-199 crystals increases as the concentration of the inner [BTC]. A wide range of crystal size can be obtained, for example, at low concentration of BTC (e.g. 0.05 mM), particles of 1  $\mu\text{m}$  are obtained in the first bands and at high concentrations (e.g. 50 mM) particles of 310  $\mu\text{m}$  are observed. The SEM images for the corresponding MOF-199 crystals are shown in Fig. 2.11.

This increase in the corresponding minimum and maximum size of the MOF-199 cubic crystals with the increase of the inner [BTC] concentration is a characteristic of the reaction-diffusion framework.

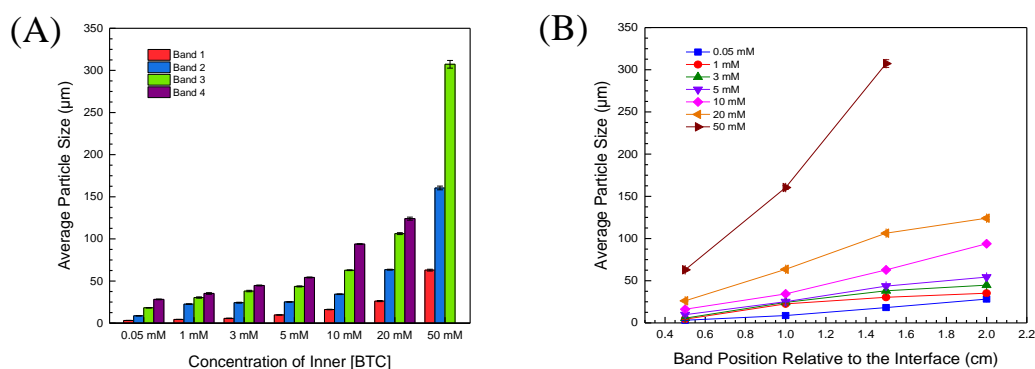


Figure 2. 10. (A) Histogram showing the variation of the average particle size ( $\mu\text{m}$ ) of MOF-199 crystals at different inner concentrations [BTC]. (B) The variation of the average particle size ( $\mu\text{m}$ ) of MOF-199 single crystals in each band as a function of the concentration of the inner [BTC].

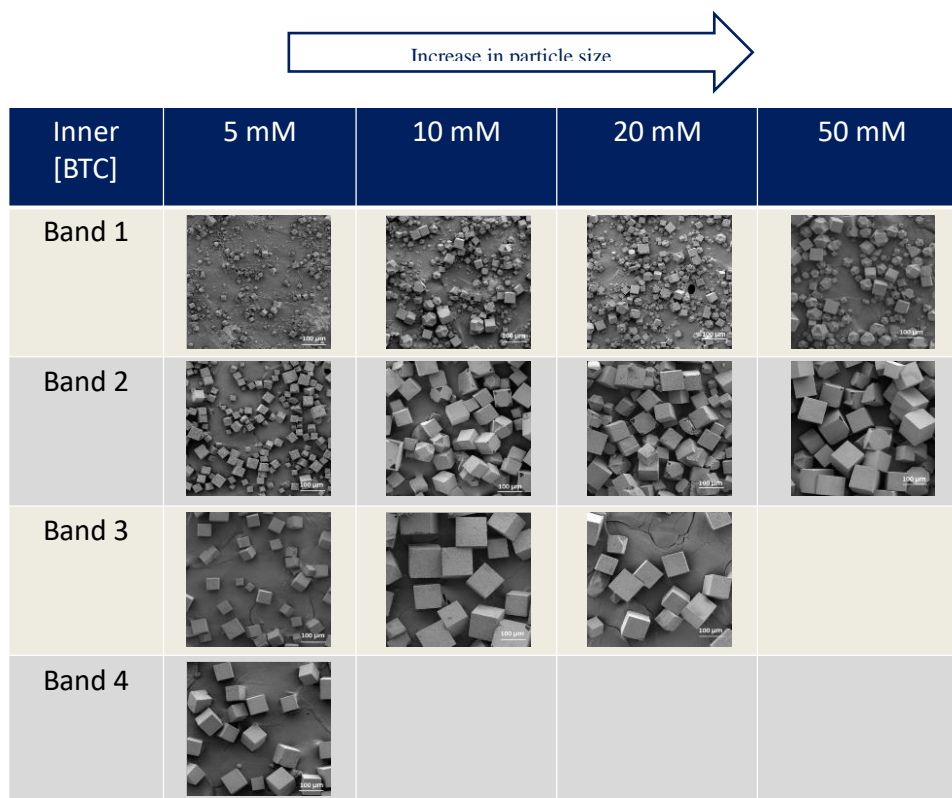


Figure 2. 11. SEM images showing the growth pattern of the MOF-199 particles at different inner [BTC] concentrations in consecutive regions of the tube (0.5cm each). Scale bar 100  $\mu\text{m}$ . Scale bar 100  $\mu\text{m}$ .

### c. Concentration of agar gel

The concentration of the agar gel was varied under four different values, 0.5%, 1%, 1.5%, and 2% while keeping the concentrations of the inner and outer constant ([BTC] 10 mM and  $[\text{Cu}(\text{OAc})_2]=100 \text{ M}$ ). The effect of the gel concentration on the growth and the crystal size was investigated. As it can be seen in Fig. 2.12 (A) and (B) and Fig 2.13., the increase in the concentration of the agar gel from 0.5% to 2%, leads to a decrease in the average particle size of the MOF-199 crystals from 30  $\mu\text{m}$  to 20  $\mu\text{m}$  in the first band and from 90  $\mu\text{m}$  to 60  $\mu\text{m}$  for the last band

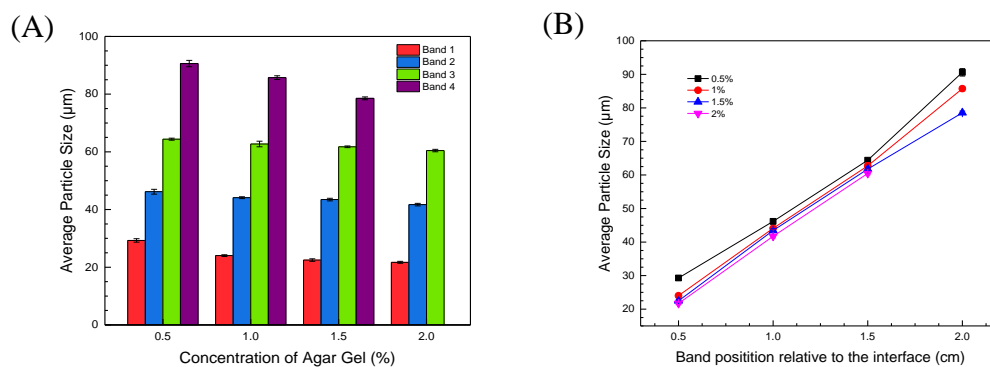


Figure 2. 12. (A) Histogram showing the variation of the average particle size of MOF-199 crystals ( $\mu\text{m}$ ) as a function of the agar gel concentration (%). (B) Plot showing the variation of the average particle size of MOF-199 crystals ( $\mu\text{m}$ ) in each band as a function of the agar gel concentration (%).

This slight decrease in the particle size of MOF-199 could be attributed to the smaller size of the gel pores at higher concentrations of the corresponding gel. On the other hand, the concentration of the gel did not affect the morphology of the MOF-199 cubic single crystals.

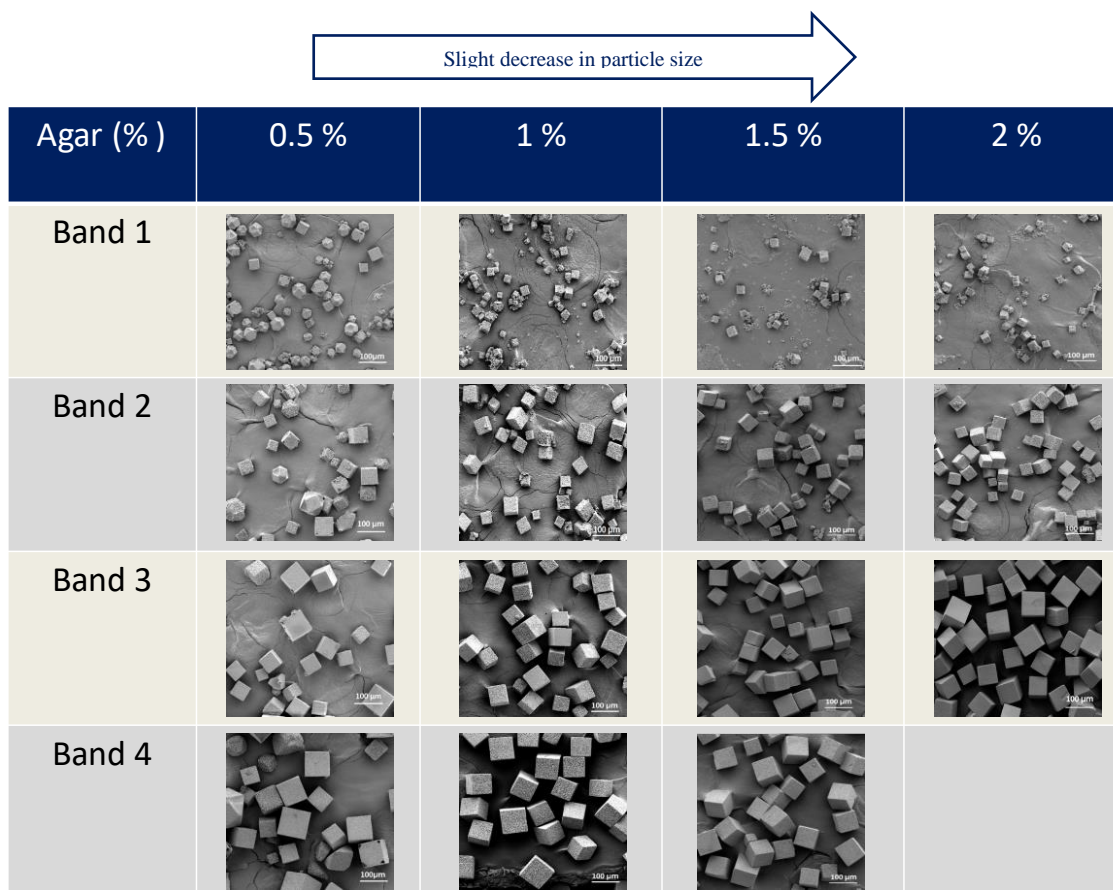


Figure 2. 13. SEM images showing the growth pattern of the MOF-199 particles at different agar gel concentration in consecutive regions of the tube (0.5cm each). Scale bar 100  $\mu\text{m}$ .

d. Copper source of the outer

In all the above experiments, we used  $\text{Cu}(\text{OAc})_2 \cdot \text{H}_2\text{O}$  as copper source in the outer part. We tested other copper sources to produce MOF-199 using RDF and we succeeded in producing single crystals in the agar gel. The PXRD patterns of the crystals obtained using  $\text{Cu}(\text{NO}_3)_2 \cdot 3\text{H}_2\text{O}$  and  $\text{CuSO}_4 \cdot 5\text{H}_2\text{O}$  in the outer as shown in Fig. 2.14, match the simulated pattern of MOF-199 and no additional peaks were observed. Nevertheless, the SEM and the microscopic images in Fig. 2.15, reveal that the MOF prepared using either  $\text{Cu}(\text{NO}_3)_2 \cdot 3\text{H}_2\text{O}$  or  $\text{CuSO}_4 \cdot 5\text{H}_2\text{O}$  in the outer is polyhedral unlike the MOF-199 prepared using  $\text{Cu}(\text{OAc})_2 \cdot \text{H}_2\text{O}$  which has a cubic morphology. In

addition, the yield of these polyhedral crystals was very low. It can be concluded from this experiment that the anions of the copper salt have a direct effect on the structure of the MOF crystals.

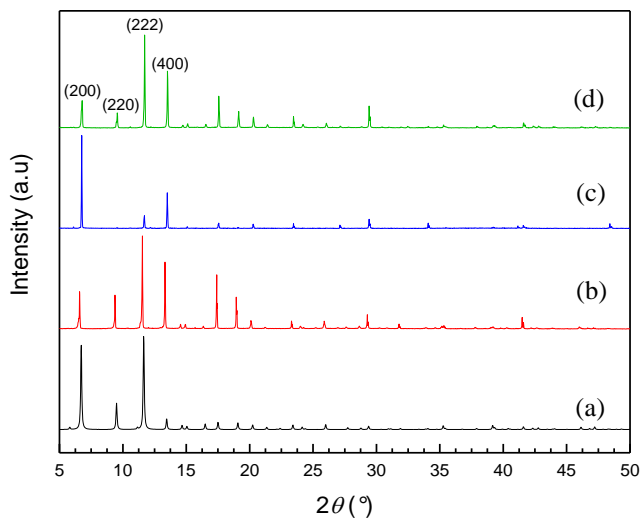


Figure 2. 14. PXRD patterns of MOF-199 synthesized by RDF using different outer as compared to the theoretical one. (a) Calculated, (b) Cu(OAc)<sub>2</sub>·H<sub>2</sub>O in the outer, (c) Cu(NO<sub>3</sub>)<sub>2</sub>·3H<sub>2</sub>O in the outer, (d) CuSO<sub>4</sub>·5H<sub>2</sub>O in the outer.



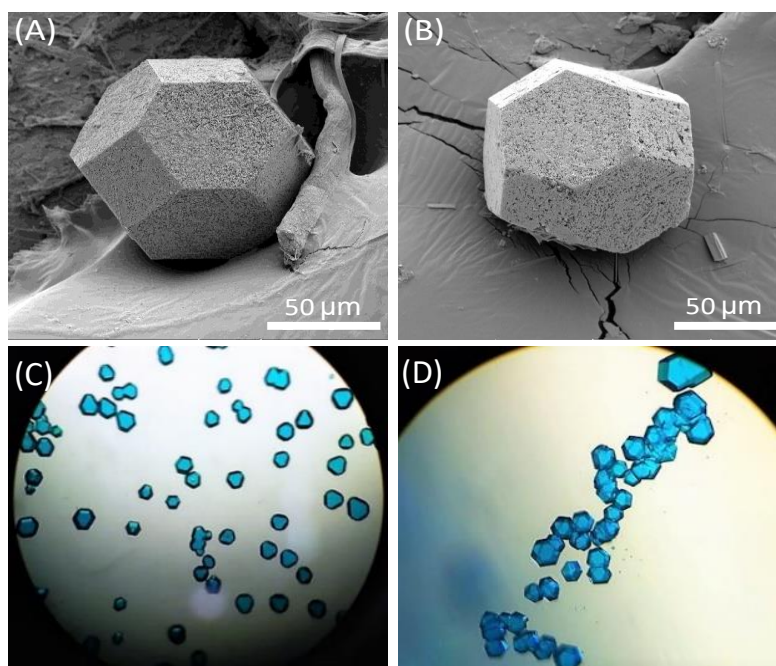


Figure 2. 15. SEM images of MOF-199 using different copper sources in the outer. (A)  $\text{Cu}(\text{NO}_3)_2 \cdot 3\text{H}_2\text{O}$ , (B)  $\text{CuSO}_4 \cdot 5\text{H}_2\text{O}$ . Microscopic images of MOF-199 using different copper sources in the outer. (C)  $\text{Cu}(\text{NO}_3)_2 \cdot 3\text{H}_2\text{O}$ , (D)  $\text{CuSO}_4 \cdot 5\text{H}_2\text{O}$ .

e. Type of the gel used in the inner

The gel network traps the crystal nuclei and prevents particles sedimentation thereby fostering a 3D growth of the crystals. Thus, the type of the gel used in RDF is an important factor in determining the size and the morphology of the MOF crystals since gels have different pore sizes within their network. Two other gels are investigated, the LB Lennox gel and the Dibenzylidene sorbitol gel (organic gel).

**LB Lennox Agar Gel:** MOF-199 sample was prepared using LB Lennox agar gel under the same conditions used the sample synthesis using the agar gel. The inner part containing the linker BTC(10 mM) was dissolved in an Ethanol/Water (50%/50%) solution, then 1% of the LB Lennox agar gel was added. The mixture is heated until the gel gets clear and directly poured into a Pyrex test tube. The tube is then covered so that the gel hardens. On the other hand, the outer part is prepared by dissolving 100 mM

$\text{Cu}(\text{OAc})_2 \cdot \text{H}_2\text{O}$  in (50%/50%) Ethanol/Water solution and it is then added to the jellified inner. The obtained precipitate was examined using PXRD and SEM. The PXRD pattern for the sample prepared using the LB Lennox agar gel is shown in Fig. 2.16 and it exactly matches the simulated MOF-199 pattern.

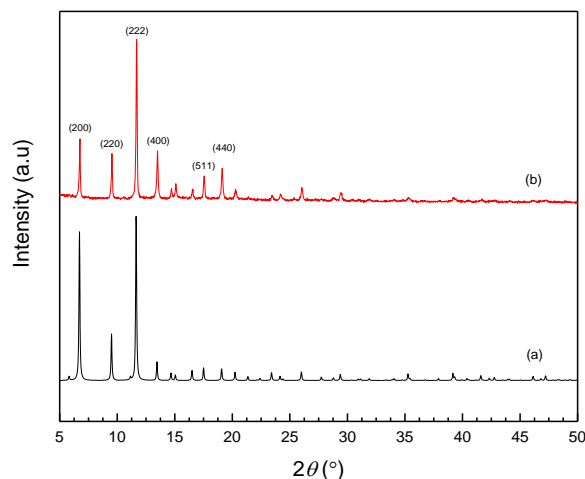


Figure 2. 16. PXRD patterns of MOF-199 (a) calculated, (b) synthesized using LB Lennox agar gel.

Moreover, the precipitate of MOF-199 obtained using the LB Lennox agar gel was divided into 4 consecutive bands each is of 0.5 cm and SEM images were taken for each band. As shown in Fig. 2.17, it is clear that the crystals obtained are not single crystals, however they look like interpenetrated cubes that are different than the single cubes obtained in the Bacto agar gel. Other than that, there is no transition or change in the crystal structure within the bands.

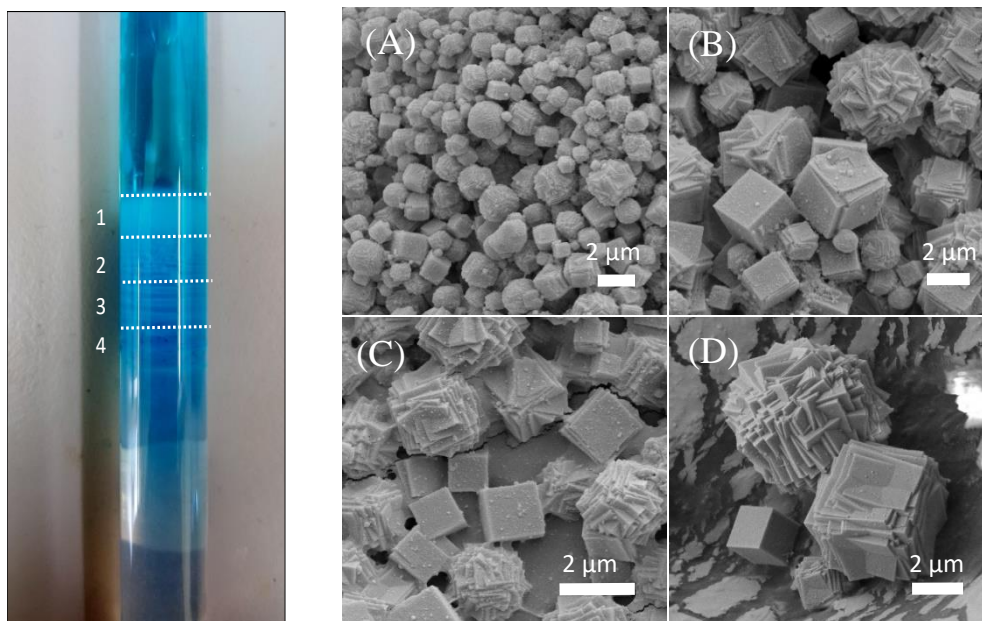


Figure 2. 17. SEM images of MOF-199 in organic gel taken at different consecutive positions from the interface. (1) Band 1, (2) Band 2, (3) Band 3, (4) Band 4, (5) Band 5.

Dibenzylidene sorbitol (DBS): MOF-199 was synthesized in Dibenzylidene sorbitol which is an organic gel by using the conditions of 10 mM BTC with 1.5% of the gel in pure ethanol solution for the inner part, and regarding the outer, 100 mM of the  $\text{Cu}(\text{OAc})_2 \cdot \text{H}_2\text{O}$  was dissolved in ethanol.

The PXRD patterns of the MOF-199 synthesized in DBS was compared to that reported in literature (Fig. 2.18). The peaks corresponding to the MOF produced in organic gel appear to be wider and have a higher full width at half maximum as compared to the one in literature. Furthermore, the diffractogram corresponding to the MOF-199 crystals in DBS appears to have a noise. This may be attributed to the very small size of these crystals. This was further confirmed by SEM imaging of the crystals.

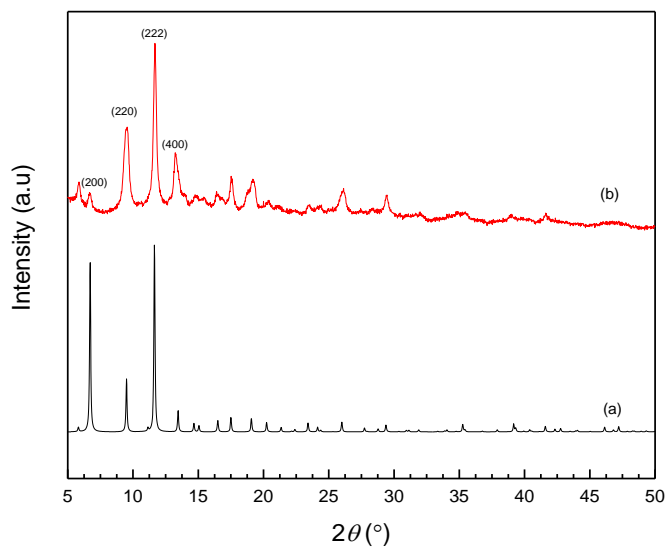


Figure 2. 18. PXRD patterns of MOF-199 (a) calculated, (b) synthesized in DBS gel.

SEM images were done on a sample separated into five consecutive bands each is of 0.5 cm. By looking at these SEM images in Fig. 2.19, it is clear that the MOF-199 samples synthesized in DBS do not have a cubic morphology. However, in the first band they appear as spheres and by going down in bands 2, 3, and 4, the spheres start to transform into the octahedral shape until reaching the final band where only pure octahedra were observed. The average particle size of the crystals obtained in each band are shown in Fig. 2.20 B . Another time, RDF synthesis method was successful in showing the transition in the morphology of the crystals as a function of distance and time as compared to other synthesis routes that lack this feature.

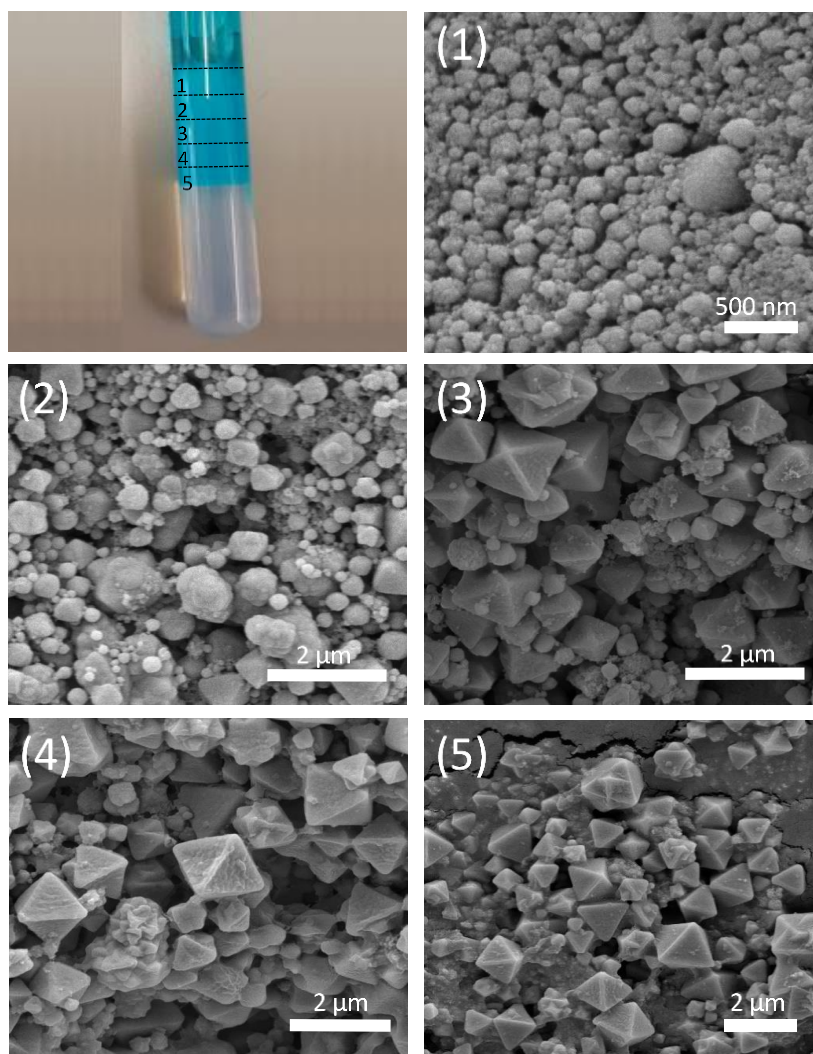


Figure 2. 19. SEM images of MOF-199 in organic gel taken at different consecutive positions from the interface. (1) Band 1, (2) Band 2, (3) Band 3, (4) Band 4, (5) Band 5.

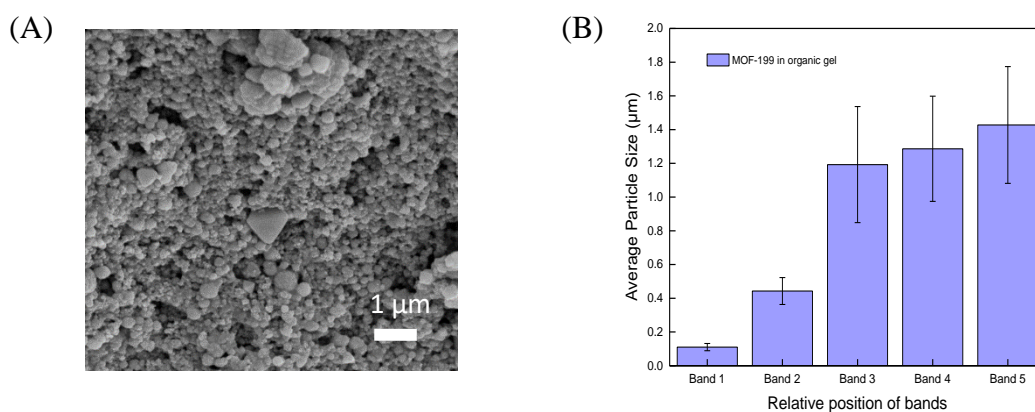


Figure 2. 20. (A) SEM images of MOF-199 spheroids produced in organic gel after 1 min from adding the outer. (B) Histogram representing the average particle size of MOF-199 synthesized in organic gel and separated into five consecutive bands (0.5 cm each).

In order to gain more understanding on the crystal growth in the DBS gel, additional kinetic studies were performed. The outer electrolyte was discarded after 1 min from adding it. The SEM image of the precipitate is shown in Fig. 2.20 (A) and it reveals that the majority of the MOF-199 crystals are small sized spheres.

In addition to that, by looking at the PXRD patterns in Fig. 2.21 corresponding to these small sized spheres, it's evidently seen that their peaks have a larger FWHM value of approximately 0.507 as compared to the larger octahedral particles having a value of 0.253. This demonstrates the formation of smaller sized particles in accordance to Scherer equation. It is noteworthy that the quality of the PXRD was not very good because of the small particle size (less than 1 μm) and the small amount of particles collected after 1 min.

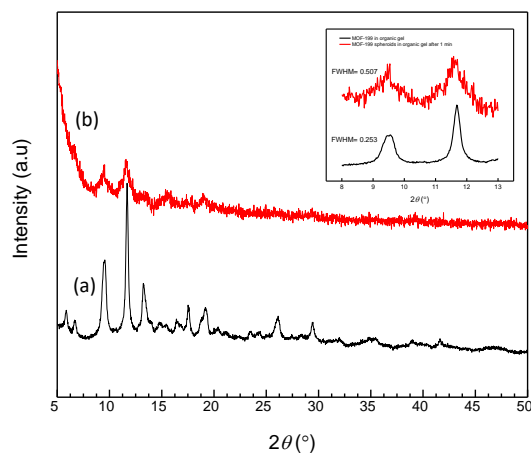


Figure 2. 21. PXRD patterns of MOF-199 synthesized in organic gel. (a) The outer was kept, (b) the outer was discarded after 1 min from adding it to the inner.

f. Reversing the components of the inner and the outer

In this case the inner and the outer are reverted where the inner consisted of 10 mM of  $\text{Cu}(\text{OAc})_2 \cdot \text{H}_2\text{O}$  and 1% agar gel in (50%/50%) EtOH/ $\text{H}_2\text{O}$ , whereas the outer consisted of 100 mM of BTC dissolved in (50%/50%) EtOH/ $\text{H}_2\text{O}$ . The formed blue precipitate is shown in Fig. 2.22. Furthermore, the SEM images of these crystals that were taken at different scales shown in Fig. 2.22 revealed that the obtained MOF has a rod-like structure with a hexagonal face.

The PXRD pattern of the crystals corresponding to the MOF in question is compared to that of MOF-199 (Fig. 2.23) and it is obvious that the two patterns do not match. This indicates the synthesized MOF has a different structure than that of MOF-199 and needs to be further investigated. Thereby, cubic MOF-199 single crystals could only form when the BTC is in the inner and the copper acetate is in the outer.

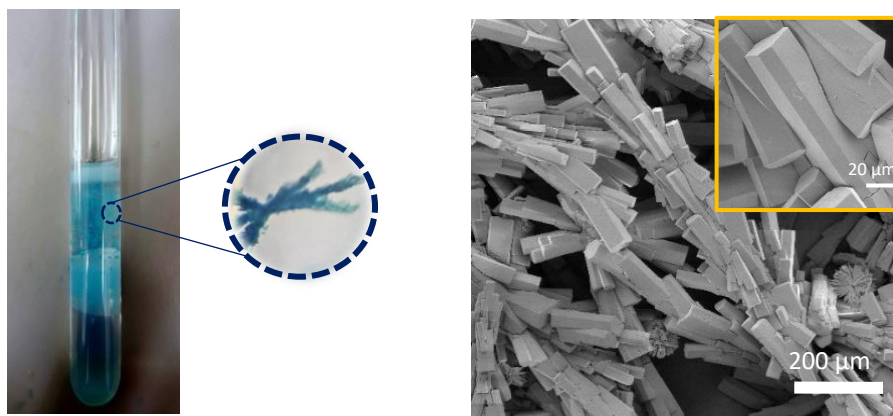


Figure 2. 22. Microscopic and SEM images of the crystals of the system composed from  $\text{Cu}(\text{OAc})_2 \cdot \text{H}_2\text{O}$  in the inner and BTC in the outer.

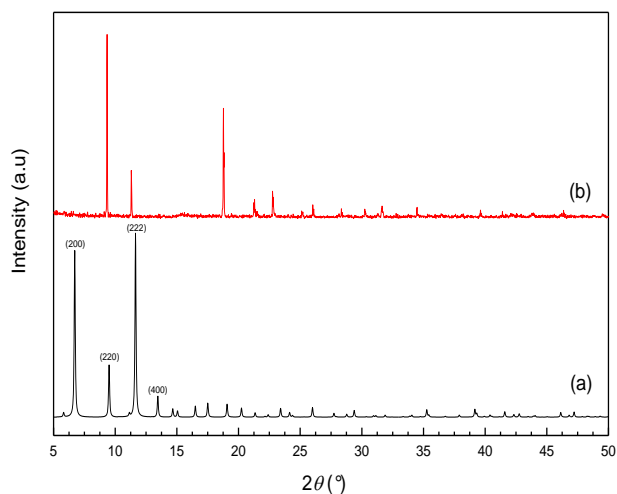


Figure 2. 23. PXRD patterns of (a) MOF-199 calculated, and (b) MOF sample under investigation.

### 7. Kinetic study and particle size analysis of MOF-199

Reaction-diffusion method in gel medium offers a suitable framework to inspect the growth and evolution of the MOF-199 single crystals owing to the substantial hampering of the nucleation and growth rates when compared to those in countless condensed media. In this context, MOF-199 is prepared in five separate



identical tubes with a known concentration of the inner and outer. Then, the formed crystals are correspondingly extracted from the inner-outer interface of each tube at different time intervals (6 s, 10 s, 5 min, 30 min and 2 h) through discarding the outer. By investigating the interface region where the nucleation dominates, the transition to the cubic MOF-199 crystals could be captured on the contrary of other synthesis method that directly yield poly-dispersed MOF-199 crystals. The morphology and the size of the MOF-199 crystals were examined using the HRSEM in Fig. 2.24, which reveals uniform nano spheroids having a maximum size of 150 nm followed by the creation of the foremost perfect MOF-199 cubic crystals after only 10 seconds from adding the outer solution. This indicates that the rates of formation and growth of the MOF-199 single crystals are very fast and superior to those reported for the solvothermal route[129]. Upon increasing the concentration of the inner [BTC], the conversion from the nano-spheroids to cubic crystals becomes too fast to be spotted. Adversely, by decreasing [BTC] a hundred fold (e.g. 0.05 mM) the initiation time extends to hours. Moreover, The PXRD pattern of MOF-199 spheroids is compared to that of the MOF-199 having cubic morphology. It is clear from Fig. 2.25 that there is no difference in the intensities of the peaks. However, the only perceptible difference is that the peaks corresponding to the spheroids (b) are broader than the ones conforming to the cubes (a) as the full width at half maximum (FWHM) of the former is greater by 2-folds of the latter. This is in agreement with Scherrer equation, which states that the smaller the crystallite size, the broader the peak gets.

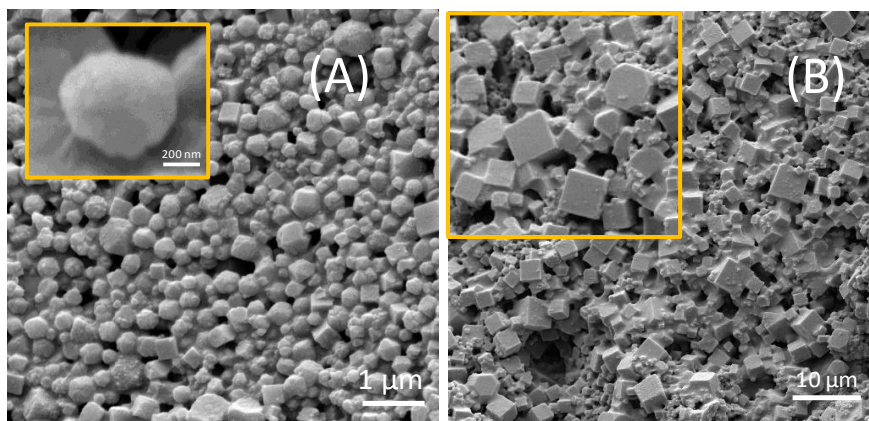


Figure 2. 24. SEM images of MOF-199 obtained after (A) 6 sec (B) 10 sec from adding the outer.

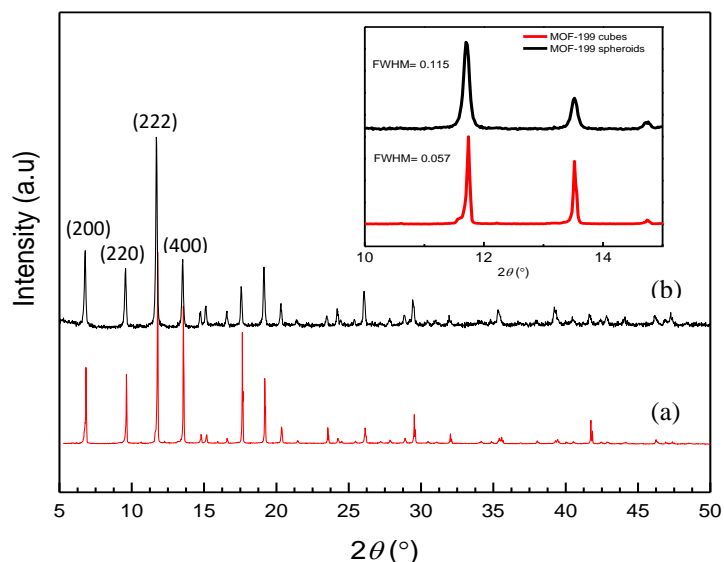


Figure 2. 25. PXRD patterns of (a) MOF-199 spheroids, (b) MOF-199 cubes.

The advantages of using the RDF method to synthesize MOF-199 are countless. Through this method, we were able to monitor and control the particle size distribution of MOF-199; this could be helpful to understand the mechanism of the reaction, which is essential for further development of the material. In addition to that, having the ability to control the size of the crystals is important for adapting MOF fabrication to a certain application. For instance, dense applications such as gas storage

require macro-sized particles, whereas particles at the nanoscale are suitable for drug delivery as they could be readily taken by the cells, they are also suitable for mixed-matrix membranes due to their facile suspension. Furthermore, the reaction occurs at room temperature, meaning that this method is cost-effective as no heat is employed. Moreover, this synthesis method is environmentally friendly since no toxic organic solvents such as DMF are used. Moreover, it is facile and produces large yields of pure single crystals within a short time.

## CHAPTER III

### SYNTHESIS OF MULTIVARIATE MOFS VIA RDF

Most of MOF structures reported to date are made from one single ligand that can be ditopic, tritopic or tetratopic. Nevertheless, MOFs incorporating more than one type of linkers (multivariate, MTV-MOFs) are rare, and their synthesis and characterization are still challenging. For the very few reported MTV-MOFs, it was demonstrated that they often display enhancement in their physical and/or chemical properties. However, the main struggle is to confirm that these organic ligands are homogeneously mixed in a single phase rather than having separate mixtures. Mainly the linkers that are mixed within the same framework have geometric similarities such as the length of the carbon chain, solubility and the functional groups. Based on our successful synthesis of MOF-199 via RDF, we investigated the possibility to incorporate another linker within the MOF-199 network by using RDF. To this end, 5-Hydroxyisophthalic acid was simultaneously added to BTC in the gel matrix. The amount of incorporated linkers within the crystals were analyzed by NMR spectroscopy which is the typical method used to characterize the mixed-linkers MOFs. The obtained MOFs are usually dissolved in acid solutions which are then subjected to  $^1\text{H}$  NMR spectroscopy. The integrals obtained from the analysis process indicate the ratios of the ligand incorporated in the crystals.

## **A. Materials and Methods**

### ***1. Materials***

Cu(OAc)<sub>2</sub>.H<sub>2</sub>O and BTC purchased from Acros Organics, Agar gel from Bacto, 5-Hydroxyisophthalic acid, N-N-Dimethyl Formamide (DMF), Dichloromethane (DCM) and Ethanol absolute from Sigma Aldrich.

### ***2. Preparation of the mixed linkers MOF and characterization***

The inner portion consists of BTC mixed with 5-Hydroxyisophthalic acid (OH-BDC) dissolved in (50%/50%) EtOH/H<sub>2</sub>O solution. After that 1% of agar gel was added and the whole reaction setup was heated near 90 °C until the gel got clear and then it was poured into a test tube to allow the jellification of the inner components. After that, the outer containing Cu(OAc)<sub>2</sub>.H<sub>2</sub>O dissolved in (50%/50%) EtOH/H<sub>2</sub>O was added to the jellified inner.

The amount of the linkers incorporated in the MOF structure is investigated using BRUKER Avance NMR Spectrometer (500 MHz) and the FT-IR spectra are recorded on Thermo Nicolet 4700 Fourier Transform Infrared Spectrometer.

## **B. Results and Discussion**

The concentration of the two linkers BTC and 5-Hydroxyisophthalic acid (OH-BDC) was varied under five different ratios (Table. 3.1):

Experiments		
I	30 mM	10 mM
II	10 mM	10 mM
III	10 mM	30 mM
IV	0 mM	10 mM
V	10 mM	0 mM

Table 3. 1. Table showing the mixed-linker MOFs prepared using different proportions of the organic linkers BTC and 5-Hydroxyisophthalic acid.

***1. Influence of the variation of the proportion of the linkers BTC and 5-Hydroxyisophthalic acid on the purity of the obtained MOF***

A blue precipitate similar to MOF-199 was obtained in 4 of the 5 tubes used. Interestingly, when OH-BDC is used alone, no precipitation was observed. Which indicates that a minimum amount of BTC was needed to crystallize the MOF structure. The PXRD patterns for the mixed linkers MOF at different ratios were compared to that of MOF-199, Fig. 3.1, and it is clear that peak positions corresponding to these patterns perfectly match the theoretical MOF-199 with no additional peaks. This demonstrated that the mixed-linker MOFs obtained are pure and have a single phase regardless of the concentration or the proportions of the ligands with respect to each other. However, the PXRDs corresponding to the mixed-linker MOFs OH-BDC:BTC (1:1) and OH-BDC:BTC (3:1) exhibit a lower quality as compared to MOF-199 and OH-BDC:BTC

(1:3). This is due to the smaller particle size of the crystals of these MOFs, thereby leading to a lower number of diffraction planes and a noise appears.

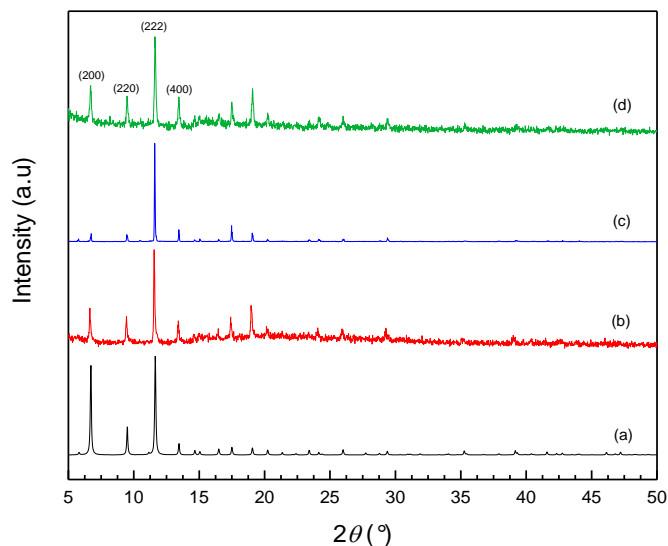


Figure 3. 1. PXRD patterns of (a) MOF-199 calculated, mixed linkers MOF containing OH-BDC:BTC (b) 1:1, (c) 1:3, (d) 3:1.

## 2. Effect of varying the ratios of the linkers on the surface area and the morphology of the MOF

The  $N_2$  adsorption isotherms for the mixed linker MOFs are shown in Fig. 3.2. The plot corresponding to the mixed linker having BTC in excess (1:3) exhibits Type I isotherm and it is similar to that of MOF-199 with a surface area of  $900 \text{ m}^2/\text{g}$ . However, as we increase the concentration of 5-Hydroxyisophthalic acid (1:1), it is evident from the plot in Fig. 3.3 (B) that a type IV isotherm is obtained, where the nitrogen uptake is high at high pressures indicating the formation of multilayers. In addition, the presence of the hysteresis loop at high relative pressures signifies the presence of micropores and mesopores. At low  $P/P_0$ , the flat plateau shows a microporous behavior and the closure of the hysteresis loop at a  $P/P_0$  value of around 0.4 shows the existence of small mesopores. The calculated surface area was  $419 \text{ m}^2/\text{g}$  which is much smaller than that

of MOF-199. By further increasing the concentration of 5-Hydroxyisophthalic acid to be in excess with respect to BTC (3:1); it is clear from the plot in Fig. 3.2 (C), that the hysteresis loop starts to disappear. This signifies that there is a change in the pore size distribution recognized by the disappearing of the micropores and a lowering in the surface area to 354 m<sup>2</sup>/g.

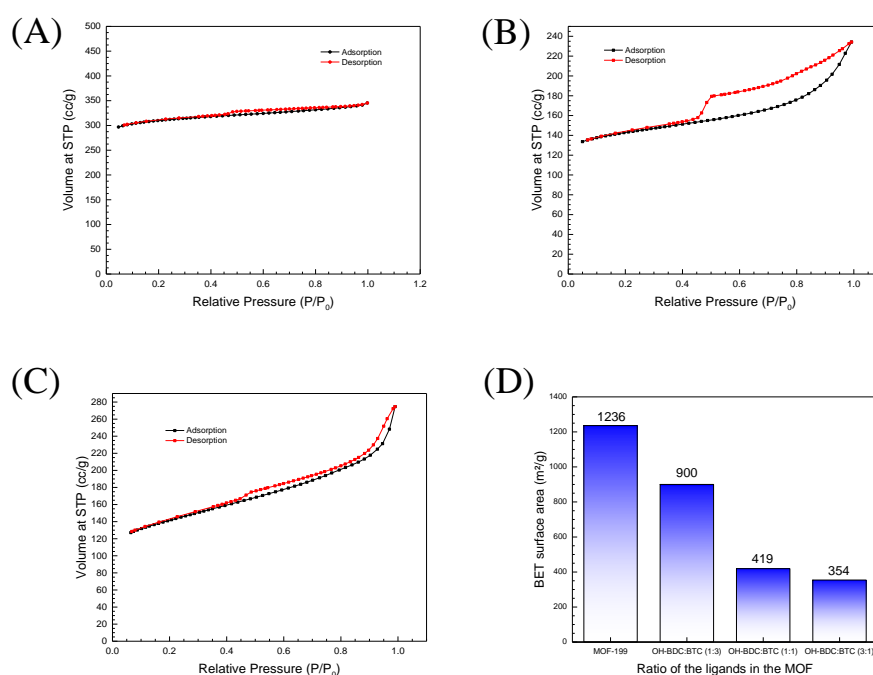


Figure 3. 2. Nitrogen physisorption isotherms of the mixed-linker MOF with OH-BDC:BTC ratios (A) 1:3, (B) 1:1, (C) 3:1, (D) Histogram showing the surface area of MOF-199, OH-BDC:BTC (1:3), OH-BDC:BTC (1:1) and OH-BDC:BTC (3:1).

These observations are further confirmed by the SEM images shown in Fig. 3.3. When the BTC was in excess with respect to OH-BDC (OH-BDC:BTC (1:3)), the obtained MOF crystals were octahedral with a smooth surface approving the nanoporous behavior in these crystals. However, when the linkers had equal concentrations (OH-BDC:BTC (1:1)), interconnected spheres were formed. The interconnection between the particles could be responsible for the mesoporous behavior of the material.



On the other hand, when the 5-Hydroxyisophthalic acid was in excess (OH-BDC:BTC (3:1)), a deformation of the spheres and a craggy surface can be observed which could explain the decrease in the surface area.

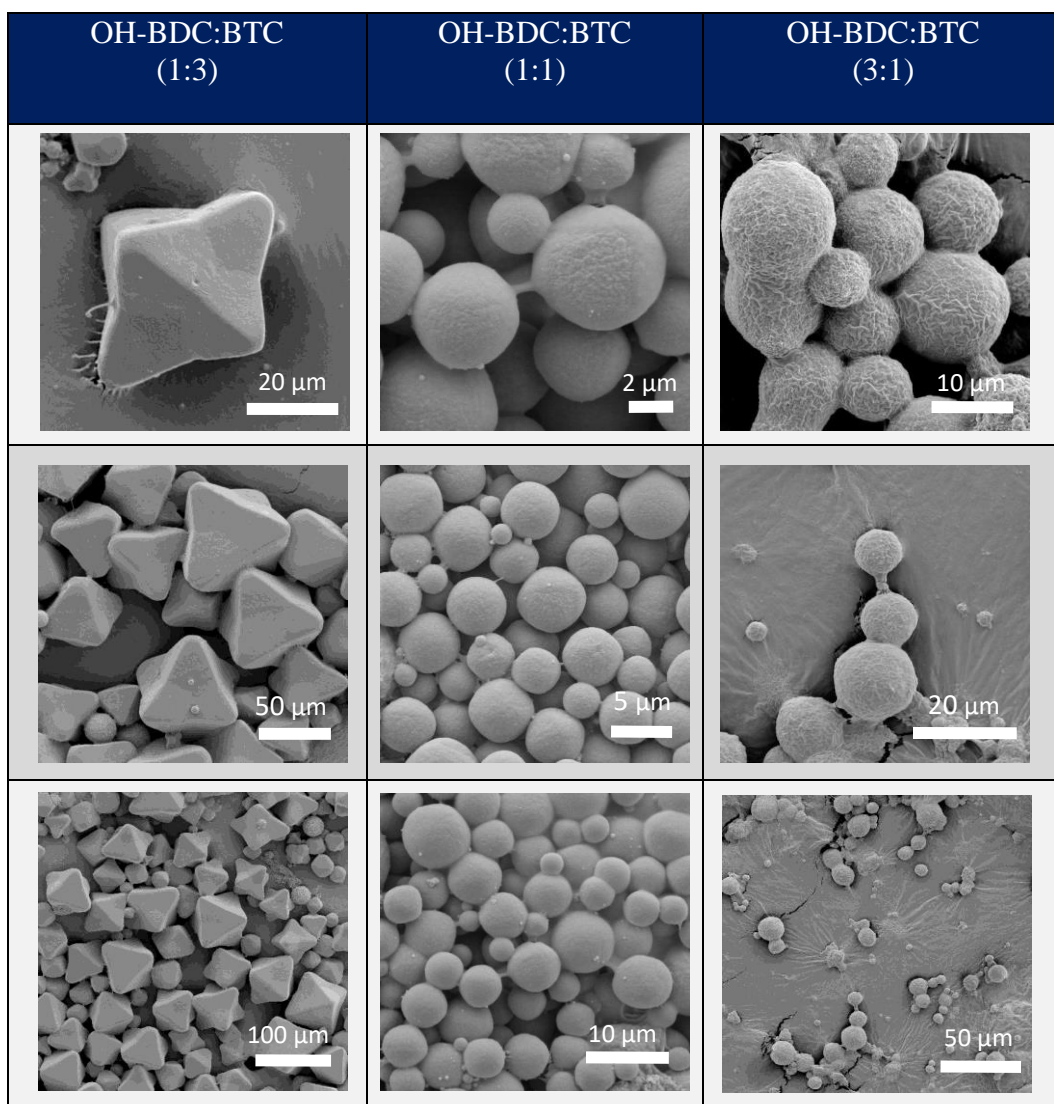


Figure 3. 3. SEM images of the mixed-linkers MOFs obtained at different proportions.

### 3. Thermal Stability of the Mixed Linkers MOF

It is clear from Fig. 3.4 that there is a slight decrease in the thermal stability of the mixed-linker MOFs prepared at different ratios of the organic linkers when compared to MOF-199. Which is consistent with the decrease in the Cu-paddle wheel SBUs within the mixed linker MOFs. Nevertheless, the TGA profiles are similar and resemble that of MOF-199 and two main weight losses are observed. The first was at around 100 °C with only 5% loss suggesting it is caused by the evaporation or the volatilization of the solvent used for washing the sample prior to analysis. The second was at around 350 °C with 47% mass loss indicating the thermal decomposition of the MOF.

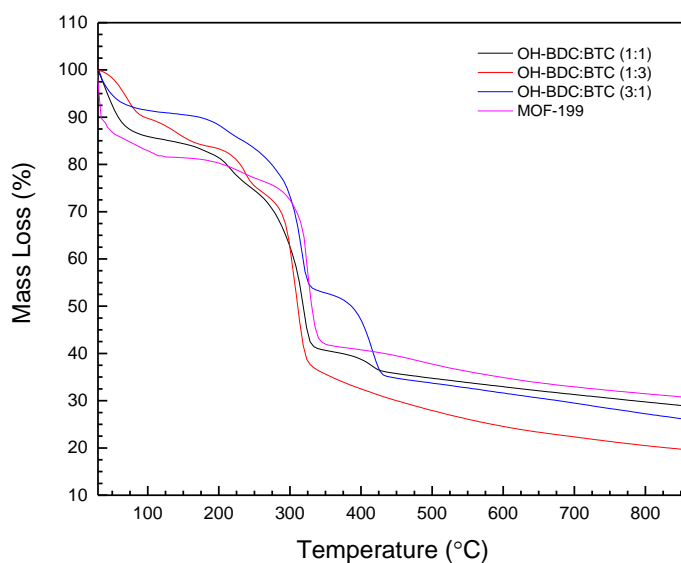


Figure 3. 4. Thermogravimetric curves of MOF-199 and mixed-linker MOFs at different proportions under nitrogen atmosphere with a heating rate of 3°C.min<sup>-1</sup> and a temperature ranging from 30 °C to 860 °C.

The FT-IR spectra of the mixed linkers MOFs at different ratios shown in Fig. 3.5. It is evident that all the IR spectra of the mixed-linkers MOFs displayed a robust stretching vibration at around 1640 cm<sup>-1</sup> corresponding to the carboxylate anions. This

attests the existence of the  $\text{-COOH}$  groups of the BTC in reaction with the copper metal ions. Whereby, the broad band appearing within  $3500\text{-}2700\text{ cm}^{-1}$  signifies the presence of free  $\text{-OH}$  groups. In addition to that, the absorption band appearing between  $500\text{-}400\text{ cm}^{-1}$  verifies the existence of the  $\text{Cu-O}$  bond. Thus, it is concluded that both linkers, BTC and 5-Hydroxyisophthalic acid are incorporated in the framework.

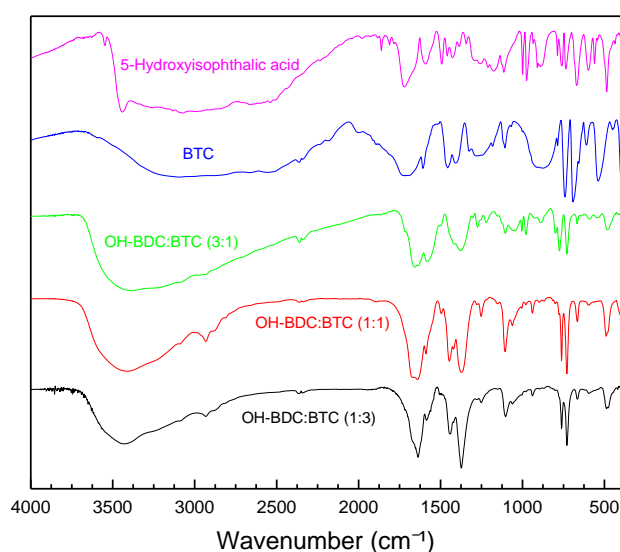


Figure 3. 5. FT-IR spectra of the mixed-linkers MOF at different ratios, BTC and 5-Hydroxyisophthalic acid.

#### 4. $^1\text{H-NMR}$ Analysis of the mixed linkers

$^1\text{H-NMR}$  Spectroscopy was very useful to quantify the amount of OH-BDC and BTC linkers incorporated within the crystals. A typical  $^1\text{H-NMR}$  spectrum is shown in Fig. 3.6, the relative amount of the ligands BTC and 5-Hydroxyisophthalic acid in the MOF can be determined. The results are illustrated in Table 3.2.

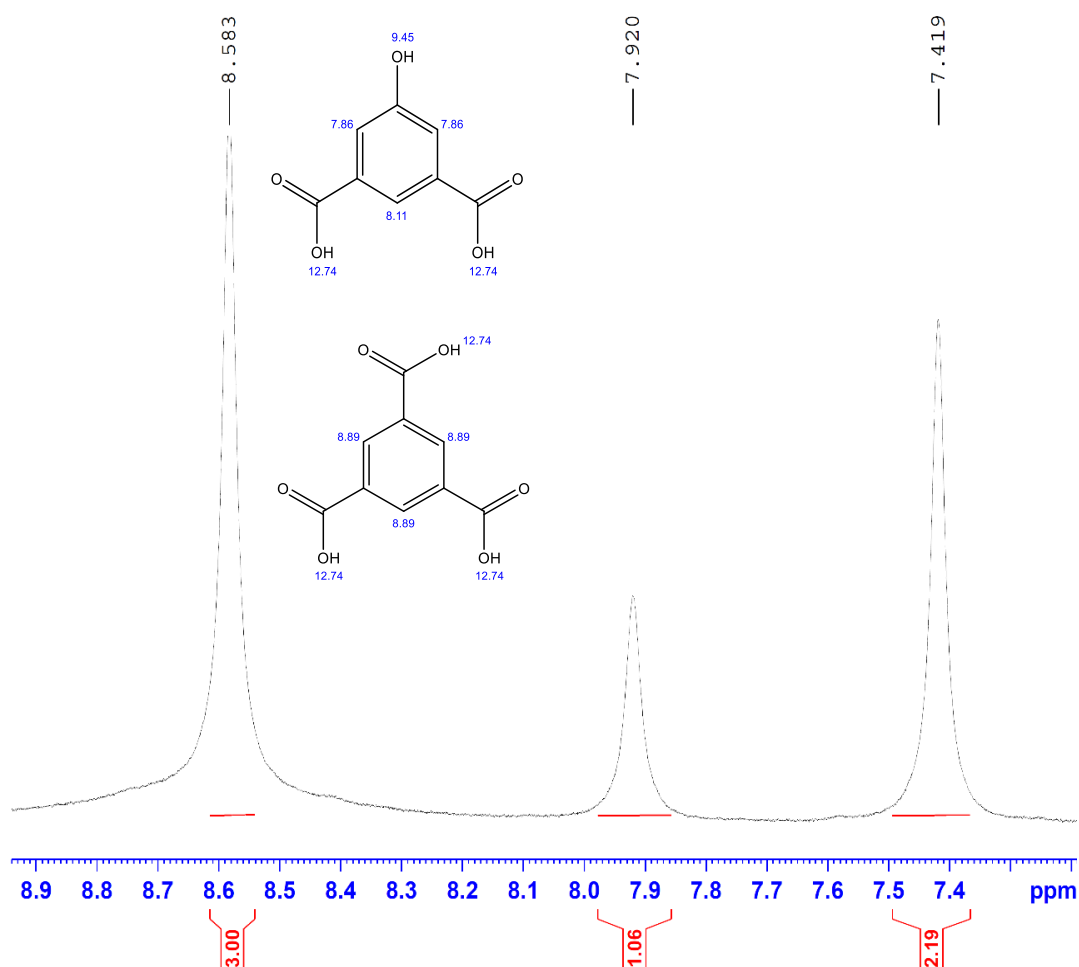


Figure 3. 6.  $^1\text{H}$ -NMR spectrum of mixed-linkers MOF OH-BDC:BTC

It is clear from Table 3.2 that the proportion of the linkers incorporated in the MOF structure is not the same as the initial proportions used in the reaction mixture. The final amount of OH-BDC was calculated to be 34.6%, 18.7% and 9.09% for initial ratios OH-BDC:BTC (3:1), (1:1) and (1:3) respectively.

Initial amount of OH-BDC incorporated in the OH-BDC:BTC MOF (%)	Amount of OH-BDC incorporated in the OH-BDC:BTC MOF (%)
25	9.09
50	18.7
75	34.6

Table 3. 2. Table showing the initial and the final amounts of the linkers OH-BDC and BTC incorporated in the MOF structure.

In this chapter, we showed that by applying RDF, two linkers have been successfully incorporated within the same framework. XRD patterns and SEM images showed the homogeneity of the prepared samples. IR and NMR demonstrated that both linkers are involved in the formation of the MOF structures. In the following chapter, we will demonstrate how useful will be the introduction of heterogeneity within order on the performance of MOFs for dye removal from water.

## CHAPTER IV

### ADSORPTION OF METHYLENE BLUE ON MOF-199 AND MIXED-LINKER MOFs

The ability of the different MOF systems reported in the previous chapters to remove methylene blue (MB) from aqueous solution has been investigated. Methylene Blue (Fig.4.1) is a cationic dye exploited in a wide range of applications including medication[130], paper coloring and dyeing wool/silk/cotton. Similar to a variety of dyes and organic pollutants, the accumulation of MB in sewage and domestic water could cause harmful effects on the ecosystem and human health, thus several endeavors were done in order to eliminate this dye in a harmless and cost-effective way[131]. In this perspective, we utilized the previously synthesized MOFs : MOF-199, OH-BDC:BTC (1:1), OH-BDC:BTC (1:3) and OH-BDC:BTC (3:1) for the removal of MB dye via adsorption process. The adsorption studies were carried out under different conditions including the initial concentration of the dye, pH of the solution, contact time and temperature. The obtained data was fitted using three different models: Langmuir, Freundlich and Tempkin isotherms. Furthermore, the mechanism of the adsorption of the dye molecules on the MOF was identified via intra-particle diffusion (Fig.4.2). Moreover, a kinetic study was carried out in which the pseudo-first order and pseudo second order kinetic models were selected and the corresponding kinetic parameters such as the rate constant, activation energy, sorption capacity at equilibrium and the correlation coefficient were estimated. It was revealed that the adsorption of Methylene Blue could be designated by the pseudo second order model. In addition, the thermodynamic parameters of the adsorption process were determined.

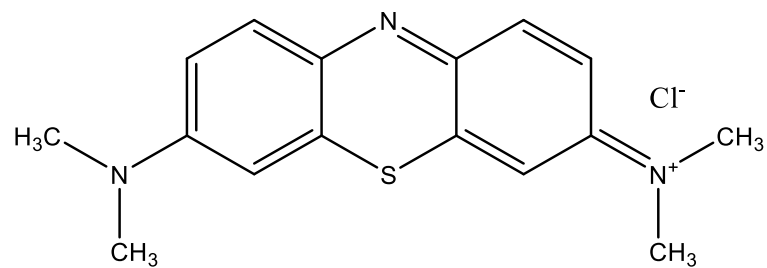


Figure 4. 1. Structure of Methylene Blue (MB)

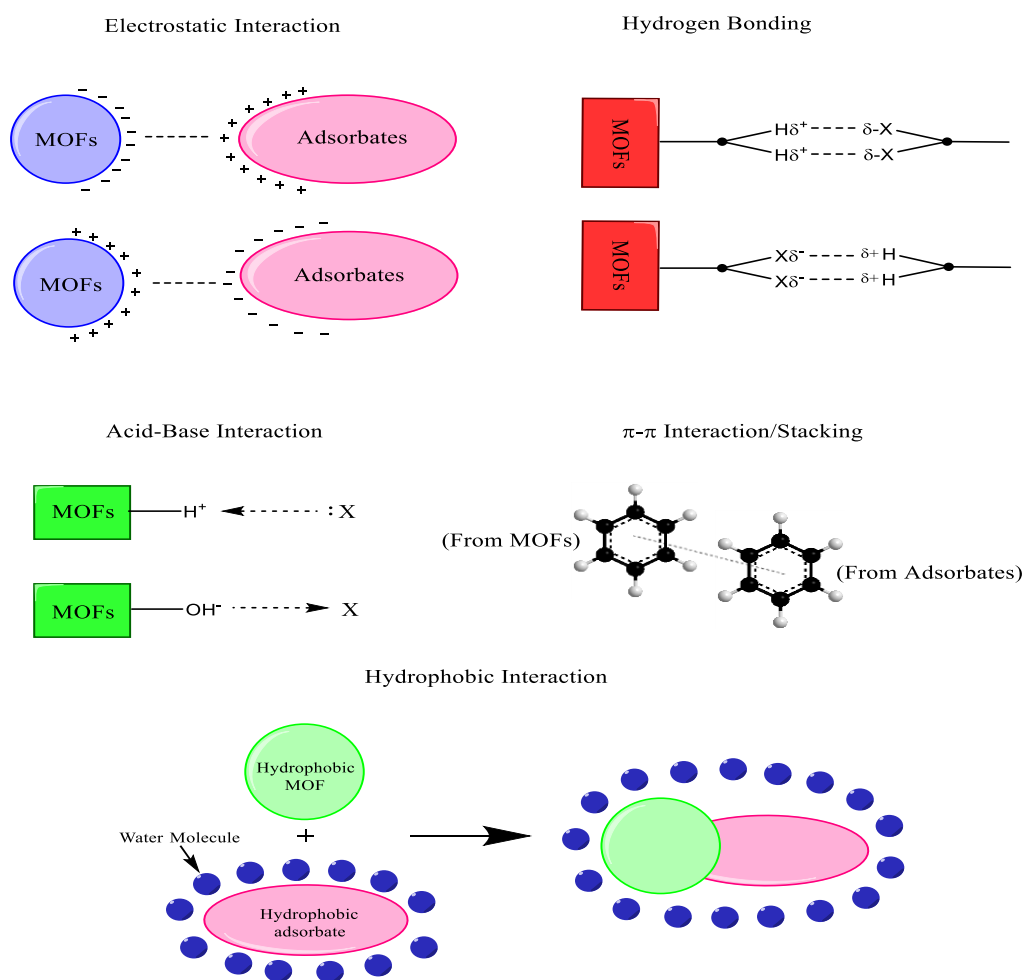


Figure 4. 2. Different adsorption mechanisms described for the adsorption of organic molecules on MOFs.

## A. Experimental Preparation

**Adsorbent:** The procedure for the preparation of the MOF systems, MOF-199 and mixed-linkers MOF with different ratios, were previously reported in chapters II and III respectively.

**Adsorbate:** The cationic dye Methylene Blue was selected for the adsorption studies. Stock solutions of 3.2 mg/L were prepared

**Adsorption Studies:** Kinetic and thermodynamic adsorption studies on MB were performed in order to investigate the adsorption performance of the different MOFs. The equilibrium adsorption experiments were accomplished by adding 10 mg of the adsorbent (MOF) into 10 mL of different initial concentrations of the dye MB. The aqueous samples were taken at different time intervals and their concentrations were calculated. The concentration determination was filtered prior to the measurement via the UV spectrophotometer “Thermo Fisher Scientific Evolution Array” set at a maximum absorption wavelength 664 nm. The amount of Methylene Blue adsorbed at equilibrium was estimated by the following equation:

$$q_e = (C_o - C_e) V/W \quad (4.1)$$

where  $C_o$  and  $C_e$  are the initial and the equilibrium concentrations (mg/L) of methylene blue respectively,  $V$  is the volume of the solution (L),  $W$  is the mass of the adsorbent (g) which is the MOF in our case study. Similarly, the amount adsorbed of methylene blue at time  $t$ , was calculated by the following equation:

$$q_t = (C_o - C_t) V/W \quad (4.2)$$

where  $C_t$  is the concentration of Methylene Blue at time  $t$ .



## **B. Results and Discussion**

The adsorption studies will be conducted at different pHs. Furthermore, a thermodynamic study will be performed at different temperatures, and different thermodynamic parameters will be estimated including the enthalpy ( $\Delta H$ ), the entropy ( $\Delta S$ ) and Gibbs-free energy ( $\Delta G$ ) will be estimated. Finally, a kinetic study will be conducted through which the order of the reaction, the rate constants and the activation energies of the MOFs are determined.

### ***1. Effect of the initial pH of the solution***

The pH of the solution is an imperative factor as it affects the transmission of the adsorbate from the aqueous solution towards the adsorbent via altering the adsorbent's surface charge. In order to examine the effect of the pH on the adsorption process, 10 mg of the adsorbent was added to 10 mL of 3.20 ppm MB dye solution in separate tubes at four different pHs (3.0, 5.0, 6.3, 8.0, 10.0) where the pH value of 6.3 corresponds to the deionized water without any additives (Fig. 4.3 (A)). The initial solution's pH was adjusted through adding 0.1M NaOH or 0.1M HCl. It is significant that the optimum pH value for the maximum removal of MB is 6.3 (de-ionized water). At low pH values (3-5), the surface of the MOF becomes positively charged due to the accumulation of the  $H^+$  ions from the solution, thereby rendering an electrostatic repulsion with the positive charge of the dye and decreasing the amount of the MB adsorbed. Likewise, at high pH values beyond 6.3, the amount of MB adsorbed on the surface of the MOF decreases, however this is due the increasing number on  $Na^+$  ions from the solution, which could compete with the cationic MB for the equivalent active adsorption sites in the MOF.

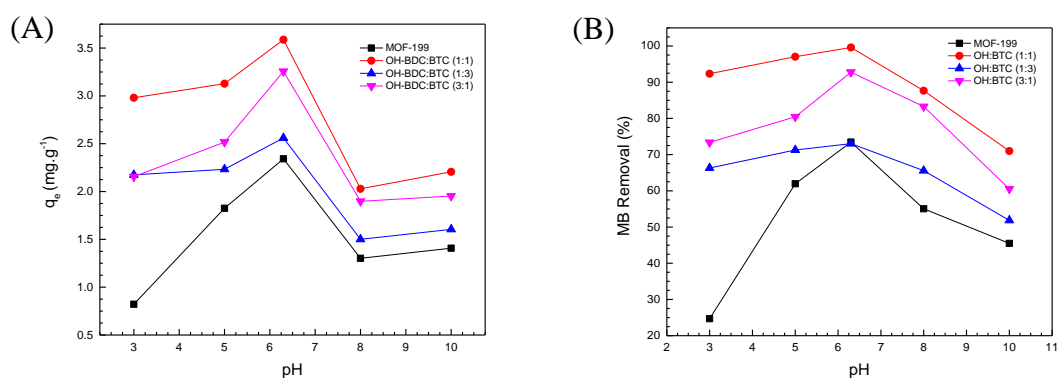


Figure 4. 3. (A) Effect of pH on the adsorption of Methylene Blue. (B) Percentage removal of Methylene Blue on the MOFs at different pHs. (Adsorption conditions: 10 mg of the MOF, 3.20 mg.L<sup>-1</sup> of the dye, 120 min contact time and 298 K).

## 2. Thermodynamic Study: Effect of temperature

In order to perceive effect of the temperature, the adsorption studies of MB onto MOF-199 and the mixed-linker MOFs were carried out at four different temperatures: 25 °C, 35 °C, 45 °C and 55 °C. The results for the thermodynamic calculations are indicated in Table 4.1. The thermodynamic parameters such as enthalpy ( $\Delta H^\circ$  kJ mol<sup>-1</sup>), entropy ( $\Delta S^\circ$  JK<sup>-1</sup> mol<sup>-1</sup>) and the Gibbs free energy ( $\Delta G^\circ$  kJ mol<sup>-1</sup>) were estimated through the Van't Hoff plot (Fig. 4.4 (A)) in accordance to the equations:

$$\Delta G = \Delta H - T\Delta S \quad (4.1)$$

$$\ln K = (\Delta S/R) - (\Delta H/RT) \quad (4.2)$$

where  $K$  is the equilibrium constant,  $R$  is the ideal gas constant (8.314 J·mol<sup>-1</sup>·K<sup>-1</sup>). The results are summarized in Table 4.1. The negative values of  $\Delta G$  signifies that the adsorption process is feasible and spontaneous. Furthermore, the increase in the magnitude of  $\Delta G$  with the rise in temperature indicates that the extent of spontaneity is escalating at higher temperatures. The second parameter is  $\Delta S$ , which reveals the disorder at the adsorbent/adsorbate interface. It is clear from Table 4.1 that the values of

$\Delta S$  are positive suggesting the high degree of disorderliness and the high affinity of the MOFs towards MB especially the mixed-linker system OH-BDC:BTC (1:1) which has the highest  $\Delta S$  value of  $265 \text{ JK}^{-1} \text{ mol}^{-1}$  as compared to OH-BDC:BTC (3:1), OH-BDC:BTC (1:3) and MOF-199 with values of 66, 60 and  $29 \text{ JK}^{-1} \text{ mol}^{-1}$  respectively. Another important parameter is the enthalpy  $\Delta H$ , which is positive for MOF-199, OH-BDC:BTC (1:1), OH-BDC:BTC (1:3) and OH-BDC:BTC (3:1) having the values 7, 73, 16 and  $17 \text{ kJ mol}^{-1}$  respectively. This demonstrates that the adsorption process is endothermic, which is in agreement with the increase of MB adsorption at higher temperatures. By comparing all the thermodynamic parameters of all of the four MOF systems, it is obvious that the MOF OH-BDC:BTC (1:1) has the uppermost values and exhibits a good adsorption performance as shown in Fig. 4.4 (B), with MB removal up to 99% superior to the other systems.

Adsorbent	$\Delta G^\circ (\text{kJ mol}^{-1})$				$\Delta H^\circ (\text{kJ mol}^{-1})$	$\Delta S^\circ (\text{JK}^{-1} \text{ mol}^{-1})$
	T=298 K	T=308 K	T=318 K	T=328 K		
MOF-199	-1.96	-2.25	-2.54	-2.83	7	29
OH-BDC:BTC (1:1)	-6.38	-9.03	-11.7	-14.3	73	265
OH-BDC:BTC (1:3)	-1.91	-2.50	-3.10	-3.69	16	60
OH-BDC:BTC (3:1)	-2.89	-3.55	-4.21	-4.88	17	66

Table 4. 1. Thermodynamic parameters of methylene blue adsorption over adsorbents at different temperatures.

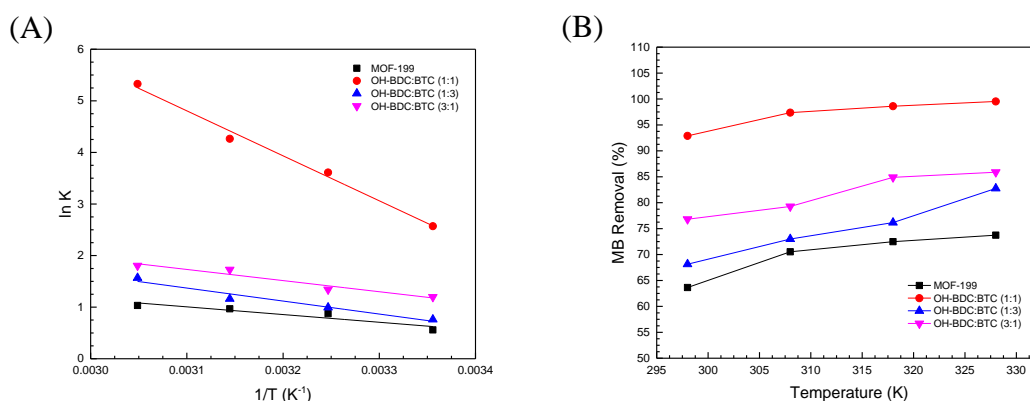


Figure 4. (A) Van't Hoff plot for the adsorption of Methylene Blue on the MOF systems. (B) Percentage removal of Methylene Blue as a function of temperature for the MOF systems.

### 3. Type of adsorption isotherm

There are various isotherms, which describe the adsorption process however, the Langmuir and Freundlich isotherms are considered the most mutual. In our study, Freundlich isotherm equation was found to have the highest  $R^2$  value as compared to other models. The plot in Fig. 4.5 is fitted in accordance to the linearized form of Freundlich equation[132]:

$$\ln q_e = \ln K_F + (1/n) \ln C_e \quad (4.3)$$

where  $q_e$  is the adsorbed amount at equilibrium ( $\text{mg}\cdot\text{g}^{-1}$ ),  $K_F$  and  $1/n$  are Freundlich constants,  $C_e$  is the concentration of the dye at equilibrium[132].  $K_F$  is an indicator of the adsorption capacity and  $1/n$  is an indicator of the adsorption intensity. It is clear from Table 4.2. that the MOF OH-BDC:BTC (1:1) has the highest value of  $K_F$  ( $11.58 \text{ mg}\cdot\text{g}^{-1}$ ) and the highest  $1/n$  value (0.89), signifying that the adsorption process is most favorable on this MOF. By having the Freundlich model as the best fit to our adsorption studies (Fig. 4.5), this proposes a physical adsorption process on the surface of the MOF.

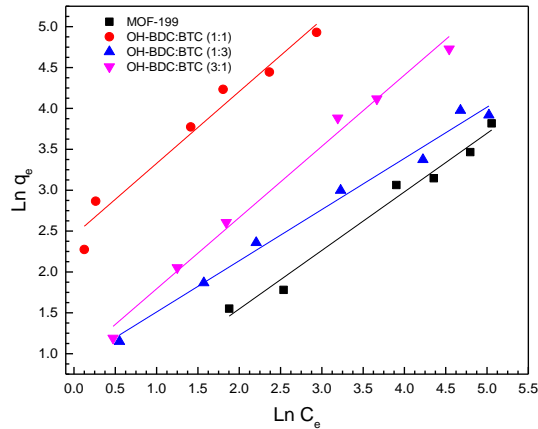


Figure 4. 5. Freundlich isotherm for Methylene Blue adsorption onto the four MOF systems.

Sample	Freundlich Isotherm		
	1/n	$K_F (L \cdot g^{-1})$	$R^2$
MOF-199	0.72	1.12	0.978
OH-BDC:BTC (1:1)	0.89	11.58	0.960
OH-BDC:BTC (1:3)	0.63	2.42	0.985
OH-BDC:BTC (3:1)	0.87	2.52	0.990

Table 4. 2. Freundlich isotherm parameters for Methylene Blue adsorption on different MOF systems.

#### 4. Kinetic Study

The adsorption study was conducted at different times (1, 3, 5, 10, 15, 25, 30, 60 and 120 minutes) from adding 10mg of the MOFs- into the 10 ml of the dye solution, each in a separate tube. The illustrations of the pseudo second order kinetic model is shown in Fig.4.6. By applying the linear regression of both kinetic models, the correlation coefficients obtained for the pseudo second order are higher than those corresponding to the pseudo first order in all of the four adsorbents as shown in Table 4.3. Therefore, it is a bimolecular reaction and the rate determining step depends on the concentration of both the adsorbent (MOF) and the adsorbate (dye).

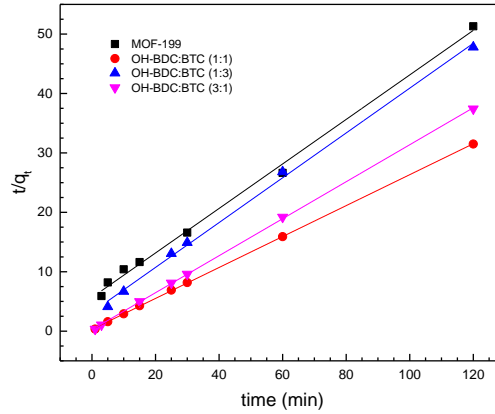


Figure 4. 6. Plot of pseudo-second order kinetic models.

Reaction Order	MOF-199	OH-BDC:BTC (1:1)	OH-BDC:BTC (1:3)	OH-BDC:BTC (3:1)
Pseudo-first order ( $R^2$ )	0.976	0.913	0.948	0.909
Pseudo-second order ( $R^2$ )	0.996	0.999	0.997	0.999

Table 4. 3. Correlation Coefficients of pseudo-first order and pseudo second-order kinetic models.

a. Adsorption Mechanism: Intra-particle diffusion

In order to gain deep understanding of the adsorption mechanism, the probability of intra-particle diffusion was investigated by applying the following equation:

$$q_t = k_{pt}^{0.5} + C \quad (4.4)$$

where  $k_p$  is the intra-particle diffusion rate constant and  $C$  is a constant that defines the boundary layer effect. The graph in Fig. 4.7 reveals that the plot is not linear over the entire time interval, though it displays a dual linearity signifying the presence of two consecutive adsorption stages of mass transport with a diminution in the rate. The first stage is the boundary layer effect whereas the second stage refers to the intra-particle diffusion, therefore a linear fit of the second stage permits the estimation of the values

of the intra-particle rate constant  $k$  and the constant  $C$ . It is known that the effect of the intra-particle diffusion is more dominant when the value of  $C$  is lower and if  $C$  reaches zero, then the adsorption process is merely controlled by intra-particle diffusion[133]. However, this is not the case as demonstrated in Fig. 4.7. It is clear that the linear plot of  $q_t$  vs  $t^{1/2}$  the of the second part didn't pass through the origin and the intercept values were 1.4, 1.5, 3 and 3.5 for MOF-199, OH-BDC:BTC (1:3), OH-BDC:BTC (3:1) and OH-BDC:BTC (1:1) respectively. This indicates that the intra-particle diffusion is not the rate-determining step and is governed by film diffusion.

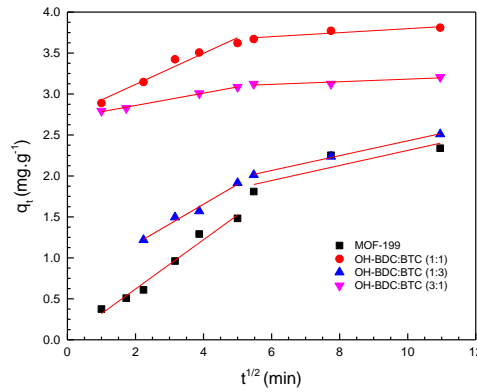


Figure 4. 7. Linear plot of intra-particle diffusion model for MOF-199, OH-BDC:BTC (1:1), OH-BDC:BTC (1:3) and OH-BDC:BTC (3:1).

#### b. Activation Energy

The linearized form of Arrhenius equation:

$$\ln k = -(E_a/RT) + \ln A \quad (4.5)$$

where  $k$  is the rate constant ( $\text{g}\cdot\text{mg}^{-1}\cdot\text{min}^{-1}$ ),  $E_a$  is the activation energy ( $\text{kJ}\cdot\text{mol}^{-1}$ ),  $R$  is the ideal gas constant ( $8.314 \text{ J}\cdot\text{mol}^{-1}\cdot\text{K}^{-1}$ ),  $T$  is the temperature (Kelvin) and  $A$  is the pre-exponential factor. It is clear from Table 4.4 that the activation energy is the lowest for the mixed-linkers MOF OH-BDC:BTC (1:1) with a value of 8.7 kJ/mol which is consistent with the highest rate constants at different temperature. Interestingly, the

activation energies for all the mixed-linkers MOFs are lower than those for the pure MOF-199.

Adsorbent	T (K)	k (g.mg <sup>-1</sup> .min <sup>-1</sup> )	1/T (K <sup>-1</sup> )	Ln k	Ea (kJ/mol)
MOF-199	298	0.0230	0.00336	-3.76	21.0
	308	0.0270	0.00325	-3.59	
	318	0.0370	0.00315	-3.28	
	328	0.0500	0.00305	-2.99	
OH-BDC:BTC (1:1)	298	0.256	0.00336	-1.36	8.70
	308	0.278	0.00325	-1.28	
	318	0.323	0.00315	-1.13	
	328	0.392	0.00305	-0.94	
OH-BDC:BTC (1:3)	298	0.0440	0.00336	-3.12	11.0
	308	0.0540	0.00325	-2.91	
	318	0.0580	0.00315	-2.85	
	328	0.0670	0.00305	-2.70	
OH-BDC:BTC (3:1)	298	0.189	0.00336	-1.66	9.30
	308	0.238	0.00325	-1.43	
	318	0.243	0.00315	-1.41	
	328	0.252	0.00305	-1.38	

Table 4. 4. Kinetic parameters for the adsorption of Methylene Blue on the MOFs.



In this chapter, we showed that the properties of the MOF could be enhanced upon introducing heterogeneity within its structure. From the results obtained, it was obvious that regardless of the proportion of the linkers in the MTV-MOF (OH-BDC:BTC), it exhibited a significant enhancement in the adsorptive activity towards MB as compared to the pure MOF-199. It was obvious that the mixed-linker MOF OH-BDC:BTC (1:1) has a good adsorption performance that vastly exceeded the other MOFs. As compared to other adsorbents reported in literature (Table 4.5), interestingly all the MOF systems that we synthesized via RDF had greater  $K_F$ , thus making these MOFs promising alternatives for the adsorption and the removal of Methylene Blue from aqueous solution.

Adsorbent	$K_F$ (L.g <sup>-1</sup> )	References
Fly Ash	0.00216	[134]
Zeolites from fly ash	0.738	[135]
Natural Zeolite	0.0537	[136]
Synthetic zeolite MCM-2	0.116	[137]
Fly ash treated with HNO <sub>3</sub>	0.0139	[138]
Surface-functionalized silica aerogel pH 8	1.443	[139]
Surface-functionalized silica aerogel pH 9	0.9552	[139]
MOF-199	1.12	This work
OH-BDC:BTC (1:1)	11.58	This work
OH-BDC:BTC (1:3)	2.42	This work
OH-BDC:BTC (3:1)	2.52	This work

Table 4. 5. Freundlich constants for the adsorption of Methylene Blue by a series of adsorbents reported in literature.

## CHAPTER V

### CONCLUSION AND FUTURE WORK

#### A. Conclusion

Herein, a novel method for the synthesis of MOFs was reported. This method is known by the reaction diffusion framework through which the organic linker is confined in a suitable gel matrix and a liquid solution of the metal salt is added on the gel matrix allowing thereby, the diffusion process and the formation of the corresponding MOF in the form of precipitate. As a proof of concept, we applied this method on the synthesis of one of the most interesting MOFs (MOF-199) which is composed of the tritopic BTC linker and copper paddle wheel SBUs. The morphology and the chemical composition of the obtained MOF crystals are subjected to characterizations using numerous analysis techniques including the XRD, BET, SEM, TGA, NMR and FT-IR. By using the RDF synthesis method, we were able to synthesize MOF-199 single crystals in large yields. The effect of temperature, concentration of the reactants and metal sources were investigated and demonstrated that these parameters affect directly the size and the morphology of the crystals. Additionally, this method allowed us to study the kinetics of the crystal growth within the gel matrix. The BET surface area of the obtained MOF-199 is 1260 m<sup>2</sup>/g, which is in agreement with the reported values. This new method of synthesizing MOFs is interesting because it is considered cost-effective, facile, rapid and environmentally friendly since water and Ethanol are the only solvents employed in the process as compared to other synthesis approaches where DMF is mainly used.

The second part involves the successful synthesis of a single phase mixed-linkers MOF which is considered as challenging process via solvothermal synthesis. In this set of new mixed linker MOFs, we successfully incorporated OH-BDC and BTC within the same frameworks. 3 Three different ratios were employed in order to study their effect on the crystal structure and the properties of the MOF. Interestingly, the OH-BDC cannot be incorporated into MOF when It is used alone under our experimental conditions. A minimum amount of BTC was needed to initiate the process. The prepared mixed-linkers MOF systems were subjected to characterizations using the same techniques used for MOF-199 including XRD, SEM, BET and IR. The extent of the incorporation of the linkers in the framework was elucidated using <sup>1</sup>H-NMR spectroscopy.

Finally, the MOF systems prepared using reaction-diffusion framework were employed in the adsorption of methylene blue dye (MB) and their adsorption performance was compared. The thermodynamic and kinetic of the adsorption process were evaluated. Interestingly, this study demonstrated that the mixed-linkers MOFs have higher affinity to MB when compared to MOF-199. And the mixed linkers MOF incorporating around 19 % of OH-BDC was the best adsorbent for MB removal from water.

## **B. Future Work**

### ***1. Synthesis of new MOFs via RDF***

We have shown that RDF can be applied to synthesize MOF-199. It would be very interesting to extend this study on the synthesis of other new MOF structures via this method. For example, this method can be potentially used to synthesize Zeolitic

Imidazolate Frameworks (ZIFs), because this subfamily of MOFs was previously synthesized at room temperature via precipitation methods. And It has been demonstrated that the size of these ZIFs crystals play a key role in many applications. By using RDF, we will be able to control the size and the morphology of the crystals and we will be able to incorporate more than one linker within the same framework. Intensive efforts have been exerted in order to synthesize a magnesium based MOF using the RDF method, however up till now none was successful. The importance of synthesizing a magnesium based MOF relies on the magnesium being lighter in weight than the copper and thus by mixing it with the copper, this leads to the enhancement of the properties of the MOF-199 and mainly its surface area. The trials that were performed in agar gel using Ethanol/H<sub>2</sub>O as the reaction solvent didn't show any precipitate. However, when using organic gel and the solvent was pure ethanol, a white precipitate appeared, though it wasn't a MOF. Accordingly, the work now should focus on optimizing the experimental conditions such as the temperature or mixing the ethanol with other organic solvents such as DMF and varying the ratio of these solvents.

## ***2. Synthesis of other mixed-metals MOFs via RDF***

We have demonstrated that by using RDF, mixed ligand MOFs can be synthesized and the amount of linkers incorporated within the crystals can be controlled. This initial finding will prompt us to study the possibility of introducing more than one metal cluster into MOFs using RDF. This could be achieved by simply adding two or more metal salts in the outer solution and hopefully by diffusion through the gel where linkers are immobilized, Mixed-metal MOFs can be produced. Magnesium is one of the potential metals that can be used in addition to copper because of its light weight

which would increase the surface area of the MOF. Initial trials that were performed in agar gel using Ethanol/H<sub>2</sub>O as the reaction solvent didn't show any precipitate.

However, when using the organic gel in ethanol, a precipitate appeared but it did not match the MOF-199 topology. More investigations are needed in order to identify the product and to optimize the experimental conditions. . Accordingly, the work now should focus on optimizing the experimental conditions such as the temperature or mixing the ethanol with other organic solvents such as DMF and varying the ratio of these solvents.

### ***3. Synthesis of other mixed-linkers MOFs***

The successful synthesis of a mixed-linker MOF using the linkers 5-Hydroxyisophthalic acid and BTC having accessible coordination sites pave the path to the synthesis of other MOFs using linkers having functional groups more reactive than the hydroxyl group such as the amino functional group (-NH<sub>2</sub>). Where post-modification reactions can be performed. These accessible functional groups are important as they could be used for further applications. For instance, the -OH group could be deprotonated into O<sup>-</sup> which in turn could be coordinated to a positively charged amino acid and generate a Bio-MOF useful for biological applications such as drug delivery.. Another important feature of synthesizing mixed-linkers MOFs using RDF systems is the ability to separate the formed precipitate into bands and follow the structure, the chemical composition and the properties in each band. This is important to investigate whether the linkers are mixed from the beginning or if there is a stage at which these linkers get incorporated. Thus, the mechanism of the formation of the MTV-MOF could be studied and explained.

## REFERENCES

1. N. Ahmad, H. A. Younus, A. H. Chughtai and F. Verpoort, *Chem Soc Rev*, 2015, **44**, 9-25.
2. O. M. Yaghi, G. Li and H. Li, *Nature*, 1995, **378**, 703.
3. M. Kondo, T. Yoshitomi, H. Matsuzaka, S. Kitagawa and K. Seki, *Angewandte Chemie International Edition in English*, 1997, **36**, 1725-1727.
4. H. Li, M. Eddaoudi, M. O'Keeffe and O. M. Yaghi, *Nature*, 1999, **402**, 276-279.
5. S. S.-Y. Chui, S. M.-F. Lo, J. P. Charmant, A. G. Orpen and I. D. Williams, *Science*, 1999, **283**, 1148-1150.
6. M. Eddaoudi, D. B. Moler, H. Li, B. Chen, T. M. Reineke, M. O'keeffe and O. M. Yaghi, *Accounts of Chemical Research*, 2001, **34**, 319-330.
7. A. Alshammari, Z. Jiang and K. E. Cordova, in *Semiconductor Photocatalysis-Materials, Mechanisms and Applications*, InTech, 2016.
8. K. Seki and W. Mori, *The Journal of Physical Chemistry B*, 2002, **106**, 1380-1385.
9. R. Haldar and T. K. Maji, *CrystEngComm*, 2013, **15**, 9276-9295.
10. C. Serre, F. Millange, C. Thouvenot, M. Noguès, G. Marsolier, D. Louër and G. Férey, *Journal of the American Chemical Society*, 2002, **124**, 13519-13526.
11. M. Eddaoudi, J. Kim, N. Rosi, D. Vodak, J. Wachter, M. O'keeffe and O. M. Yaghi, *Science*, 2002, **295**, 469-472.
12. C. Dey, T. Kundu, B. P. Biswal, A. Mallick and R. Banerjee, *Acta Crystallogr B Struct Sci Cryst Eng Mater*, 2014, **70**, 3-10.
13. H. Furukawa, K. E. Cordova, M. O'Keeffe and O. M. Yaghi, *Science*, 2013, **341**, 1230444.
14. L. E. Kreno, K. Leong, O. K. Farha, M. Allendorf, R. P. Van Duyne and J. T. Hupp, *Chem Rev*, 2012, **112**, 1105-1125.
15. C. V. McGuire and R. S. Forgan, *Chem Commun (Camb)*, 2015, **51**, 5199-5217.
16. A. J. Howarth, Y. Liu, P. Li, Z. Li, T. C. Wang, J. T. Hupp and O. K. Farha, *Nature Reviews Materials*, 2016, **1**, 15018.
17. O. M. Yaghi, M. O'Keeffe, N. W. Ockwig, H. K. Chae, M. Eddaoudi and J. Kim, *Nature*, 2003, **423**, 705-714.
18. A. Macchioni, *Chemical reviews*, 2005, **105**, 2039-2074.
19. X. Huang, Y. Chen, Z. Lin, X. Ren, Y. Song, Z. Xu, X. Dong, X. Li, C. Hu and B. Wang, *Chemical Communications*, 2014, **50**, 2624-2627.
20. V. I. Isaeva, E. V. Belyaeva, A. N. Fitch, V. V. Chernyshev, S. N. Klyamkin and L. M. Kustov, *Crystal Growth & Design*, 2013, **13**, 5305-5315.
21. H. Furukawa, K. E. Cordova, M. O'Keeffe and O. M. Yaghi, *Science*, 2013, **341**, 1230444.
22. R. Haldar and T. K. Maji, *CrystEngComm*, 2013, **15**, 9276-9295.
23. X. Kong, H. Deng, F. Yan, J. Kim, J. A. Swisher, B. Smit, O. M. Yaghi and J. A. Reimer, *Science*, 2013, **341**, 882-885.
24. J.-S. Qin, S. Yuan, Q. Wang, A. Alsalmé and H.-C. Zhou, *Journal of Materials Chemistry A*, 2017, **5**, 4280-4291.
25. T. M. Osborn Popp and O. M. Yaghi, *Accounts of Chemical Research*, 2017, **50**, 532-534.

26. H. Furukawa, U. Müller and O. M. Yaghi, *Angewandte Chemie International Edition*, 2015, **54**, 3417-3430.
27. T. Ben, C. Pei, D. Zhang, J. Xu, F. Deng, X. Jing and S. Qiu, *Energy & Environmental Science*, 2011, **4**, 3991-3999.
28. W. Kleist, F. Jutz, M. Maciejewski and A. Baiker, *European Journal of Inorganic Chemistry*, 2009, **2009**, 3552-3561.
29. N. Stock and S. Biswas, *Chemical reviews*, 2011, **112**, 933-969.
30. D. J. Tranchemontagne, J. R. Hunt and O. M. Yaghi, *Tetrahedron*, 2008, **64**, 8553-8557.
31. A. Pichon, A. Lazuen-Garay and S. L. James, *CrystEngComm*, 2006, **8**, 211-214.
32. J. Klinowski, F. A. A. Paz, P. Silva and J. Rocha, *Dalton transactions*, 2011, **40**, 321-330.
33. C. G. Carson, A. J. Brown, D. S. Sholl and S. Nair, *Crystal Growth & Design*, 2011, **11**, 4505-4510.
34. C. McKinstry, R. J. Cathcart, E. J. Cussen, A. J. Fletcher, S. V. Patwardhan and J. Sefcik, *Chemical Engineering Journal*, 2016, **285**, 718-725.
35. C. Hardacre and V. Parvulescu, *Catalysis in Ionic Liquids: From Catalyst Synthesis to Application*, Royal Society of Chemistry, 2014.
36. M. G. Clerici and O. A. Kholdeeva, *Liquid phase oxidation via heterogeneous catalysis: organic synthesis and industrial applications*, John Wiley & Sons, 2013.
37. S. R. Caskey and A. J. Matzger, *Mater. Matters*, 2009, **4**, 111.
38. S. Wang, W. Morris, Y. Liu, C. M. McGuirk, Y. Zhou, J. T. Hupp, O. K. Farha and C. A. Mirkin, *Angewandte Chemie*, 2015, **127**, 14951-14955.
39. T. Frišćić, *Encyclopedia of Inorganic and Bioinorganic Chemistry*, 2011.
40. A. Pichon, A. Lazuen-Garay and S. L. James, *CrystEngComm*, 2006, **8**, 211-214.
41. B. Chen and G. Qian, *Metal-organic frameworks for photonics applications*, Springer, 2014.
42. M. Klimakow, P. Klobes, A. F. Thünemann, K. Rademann and F. Emmerling, *Chemistry of Materials*, 2010, **22**, 5216-5221.
43. T. Friscic, I. Halasz, P. J. Beldon, A. M. Belenguer, F. Adams, S. A. Kimber, V. Honkimaki and R. E. Dinnebier, *Nat Chem*, 2013, **5**, 66-73.
44. D. R. Weyna, T. Shattock, P. Vishweshwar and M. J. Zaworotko, *Crystal Growth and Design*, 2009, **9**, 1106-1123.
45. H. Zhang, J. Zhong, G. Zhou, J. Wu, Z. Yang and X. Shi, *Journal of Nanomaterials*, 2016, **2016**.
46. A. Majedi, F. Davar and A. Abbasi, *International Journal of Nano Dimension*, 2016, **7**, 1.
47. Z. Ni and R. I. Masel, *Journal of the American Chemical Society*, 2006, **128**, 12394-12395.
48. R. Hoogenboom, M. W. Fijten, H. M. Thijs, B. M. van Lankvelt and U. S. Schubert, *Designed monomers and polymers*, 2005, **8**, 659-671.
49. S. Sachdeva, A. Pustovarenko, E. J. Sudhölter, F. Kapteijn, L. C. de Smet and J. Gascon, *CrystEngComm*, 2016, **18**, 4018-4022.
50. L. Fotouhi and M. Naseri, *Critical Reviews in Analytical Chemistry*, 2016, **46**, 323-331.

51. H. Al-Kutubi, J. Gascon, E. J. Sudhölter and L. Rassaei, *ChemElectroChem*, 2015, **2**, 462-474.
52. M. Lanchas, S. Arcediano, G. Beobide, O. Castillo, A. Luque and S. Perez-Yanez, *Inorganic Chemistry Frontiers*, 2015, **2**, 425-433.
53. A. Martinez Joaristi, J. Juan-Alcañiz, P. Serra-Crespo, F. Kapteijn and J. Gascon, *Crystal Growth & Design*, 2012, **12**, 3489-3498.
54. S. Dharmarathna, C. K. King'ondeu, W. Pedrick, L. Pahalagedara and S. L. Suib, *Chemistry of Materials*, 2012, **24**, 705-712.
55. R. Gupta, A. Basile and T. Veziroglu, *Journal*, 2015.
56. M. Y. Masoomi, A. Morsali and P. C. Junk, *RSC Advances*, 2014, **4**, 47894-47898.
57. W.-J. Son, J. Kim, J. Kim and W.-S. Ahn, *Chemical Communications*, 2008, DOI: 10.1039/B814740J, 6336-6338.
58. T. J. Mason and D. Peters, *Practical sonochemistry: Power ultrasound uses and applications*, Woodhead Publishing, 2002.
59. A. Burrows, C. Lamberti, E. Pidko, I. L. Minguez, D. de Vos, J. T. Hupp, J. Juan-Alcaniz, H. García, R. Palkovits and F. Kapteijn, *Metal organic frameworks as heterogeneous catalysts*, Royal Society of Chemistry, 2013.
60. K. S. Suslick, T. Hyeon and M. Fang, *Chemistry of materials*, 1996, **8**, 2172-2179.
61. Z.-Q. Li, L.-G. Qiu, T. Xu, Y. Wu, W. Wang, Z.-Y. Wu and X. Jiang, *Materials Letters*, 2009, **63**, 78-80.
62. H. Uehara, S. p. Diring, S. Furukawa, Z. Kalay, M. Tsotsalas, M. Nakahama, K. Hirai, M. Kondo, O. Sakata and S. Kitagawa, *Journal of the American Chemical Society*, 2011, **133**, 11932-11935.
63. S. Diring, S. Furukawa, Y. Takashima, T. Tsuruoka and S. Kitagawa, *Chemistry of Materials*, 2010, **22**, 4531-4538.
64. M. Y. Masoomi, S. Beheshti and A. Morsali, *Crystal Growth & Design*, 2015, **15**, 2533-2538.
65. C. Wang, X. Liu, N. K. Demir, J. P. Chen and K. Li, *Chemical Society Reviews*, 2016, **45**, 5107-5134.
66. M. Sindoro, N. Yanai, A.-Y. Jee and S. Granick, *Accounts of chemical research*, 2013, **47**, 459-469.
67. S. Rojas, F. J. Carmona, C. R. Maldonado, P. Horcajada, T. Hidalgo, C. Serre, J. A. Navarro and E. Barea, *Inorganic chemistry*, 2016, **55**, 2650-2663.
68. D. Zhao, Y. Cui, Y. Yang and G. Qian, *CrystEngComm*, 2016, **18**, 3746-3759.
69. X. Yang and Q. Xu, *Crystal Growth & Design*, 2017, **17**, 1450-1455.
70. G. Xiong, B. Yu, J. Dong, Y. Shi, B. Zhao and L.-N. He, *Chemical Communications*, 2017, **53**, 6013-6016.
71. J. Lee, O. K. Farha, J. Roberts, K. A. Scheidt, S. T. Nguyen and J. T. Hupp, *Chemical Society Reviews*, 2009, **38**, 1450-1459.
72. A. H. Chughtai, N. Ahmad, H. A. Younus, A. Laypkov and F. Verpoort, *Chemical Society Reviews*, 2015, **44**, 6804-6849.
73. R. Kitaura, G. Onoyama, H. Sakamoto, R. Matsuda, S. i. Noro and S. Kitagawa, *Angewandte Chemie*, 2004, **116**, 2738-2741.
74. P. Valvekens, F. Vermoortele and D. De Vos, *Catalysis Science & Technology*, 2013, **3**, 1435-1445.



75. A. Clearfield and Z. Wang, *Journal of the Chemical Society, Dalton Transactions*, 2002, 2937-2947.
76. O. R. Evans, H. L. Ngo and W. Lin, *Journal of the American Chemical Society*, 2001, **123**, 10395-10396.
77. T. Sawaki and Y. Aoyama, *Journal of the American Chemical Society*, 1999, **121**, 4793-4798.
78. B. Gomez-Lor, E. Gutierrez-Puebla, M. Iglesias, M. Monge, C. Ruiz-Valero and N. Snejkó, *Inorganic chemistry*, 2002, **41**, 2429-2432.
79. J. Zheng, X. Liu, P. Xu, P. Liu, Y. Zhao and J. Yang, *International Journal of Hydrogen Energy*, 2012, **37**, 1048-1057.
80. C. E. Wilmer, O. K. Farha, T. Yildirim, I. Eryazici, V. Krungleviciute, A. A. Sarjeant, R. Q. Snurr and J. T. Hupp, *Energy & Environmental Science*, 2013, **6**, 1158-1163.
81. N. Chouhan, R.-S. Liu and J. Zhang, *Photochemical Water Splitting: Materials and Applications*, CRC Press, 2017.
82. J. L. Rowsell and O. M. Yaghi, *Angewandte Chemie International Edition*, 2005, **44**, 4670-4679.
83. S. Yang, X. Lin, A. J. Blake, G. S. Walker, P. Hubberstey, N. R. Champness and M. Schröder, *Nature chemistry*, 2009, **1**, 487-493.
84. Y. Li and R. T. Yang, *Langmuir*, 2007, **23**, 12937-12944.
85. L. J. Murray, M. Dinca and J. R. Long, *Chemical Society Reviews*, 2009, **38**, 1294-1314.
86. R. Vaidhyanathan, S. S. Iremonger, K. W. Dawson and G. K. Shimizu, *Chemical communications*, 2009, 5230-5232.
87. A. Torrisi, R. G. Bell and C. Mellot-Draznieks, *Crystal Growth & Design*, 2010, **10**, 2839-2841.
88. T. C. Wang, W. Bury, D. A. Gómez-Gualdrón, N. A. Vermeulen, J. E. Mondloch, P. Deria, K. Zhang, P. Z. Moghadam, A. A. Sarjeant and R. Q. Snurr, *Journal of the American Chemical Society*, 2015, **137**, 3585-3591.
89. H. Furukawa, N. Ko, Y. B. Go, N. Aratani, S. B. Choi, E. Choi, A. Ö. Yazaydin, R. Q. Snurr, M. O'Keeffe and J. Kim, *Science*, 2010, **329**, 424-428.
90. H. Wu, W. Zhou and T. Yildirim, *Journal of the American Chemical Society*, 2009, **131**, 4995-5000.
91. Z. Xiang, Z. Hu, D. Cao, W. Yang, J. Lu, B. Han and W. Wang, *Angewandte Chemie International Edition*, 2011, **50**, 491-494.
92. Y. Cui, Y. Yue, G. Qian and B. Chen, *Chemical reviews*, 2011, **112**, 1126-1162.
93. D. Farrusseng, *Metal-organic frameworks: applications from catalysis to gas storage*, John Wiley & Sons, 2011.
94. L. Meyer, F. Schönfeld and K. Müller-Buschbaum, *Chemical Communications*, 2014, **50**, 8093-8108.
95. J. Rong, W. Zhang and J. Bai, *CrystEngComm*, 2016, **18**, 7728-7736.
96. F. Liu, L. Zhang, R. Wang, J. Sun, J. Yang, Z. Chen, X. Wang and D. Sun, *CrystEngComm*, 2014, **16**, 2917-2928.
97. S. Keskin and S. Kızılel, *Industrial & Engineering Chemistry Research*, 2011, **50**, 1799-1812.
98. I. Erucar and S. Keskin, *Industrial & Engineering Chemistry Research*, 2016, **55**, 1929-1939.

99. R. C. Huxford, J. Della Rocca and W. Lin, *Current opinion in chemical biology*, 2010, **14**, 262-268.
100. Z. Moussa, M. Hmadeh, M. G. Abiad, O. H. Dib and D. Patra, *Food chemistry*, 2016, **212**, 485-494.
101. P. Horcajada, C. Serre, M. Vallet-Regí, M. Sebban, F. Taulelle and G. Férey, *Angewandte chemie*, 2006, **118**, 6120-6124.
102. T. Faust, *Nature chemistry*, 2015, **7**, 270.
103. W. Cai, C. C. Chu, G. Liu and Y. X. J. Wáng, *Small*, 2015, **11**, 4806-4822.
104. F. Ke, L.-G. Qiu, Y.-P. Yuan, F.-M. Peng, X. Jiang, A.-J. Xie, Y.-H. Shen and J.-F. Zhu, *Journal of hazardous materials*, 2011, **196**, 36-43.
105. N. A. Khan, Z. Hasan and S. H. Jhung, *Journal of hazardous materials*, 2013, **244**, 444-456.
106. Y. Wang, G. Ye, H. Chen, X. Hu, Z. Niu and S. Ma, *Journal of Materials Chemistry A*, 2015, **3**, 15292-15298.
107. H. S. Rai, M. S. Bhattacharyya, J. Singh, T. Bansal, P. Vats and U. Banerjee, *Critical reviews in environmental science and technology*, 2005, **35**, 219-238.
108. S. Lin, Z. Song, G. Che, A. Ren, P. Li, C. Liu and J. Zhang, *Microporous and Mesoporous Materials*, 2014, **193**, 27-34.
109. A. A. Adeyemo, I. O. Adeoye and O. S. Bello, *Toxicological & Environmental Chemistry*, 2012, **94**, 1846-1863.
110. E. Haque, J. W. Jun and S. H. Jhung, *J Hazard Mater*, 2011, **185**, 507-511.
111. B. A. Grzybowski, *Chemistry in motion: reaction-diffusion systems for micro- and nanotechnology*, John Wiley & Sons, 2009.
112. M. Al-Ghoul, R. Issa and M. Hmadeh, *CrystEngComm*, 2017.
113. G. A. Al Akhrass, M. Ammar, H. El-Rassy and M. Al-Ghoul, *RSC Advances*, 2016, **6**, 3433-3439.
114. J. Rahbani, M. Ammar and M. Al-Ghoul, *The Journal of Physical Chemistry A*, 2013, **117**, 1685-1691.
115. E. L. Cussler, *Diffusion: mass transfer in fluid systems*, Cambridge university press, 2009.
116. A. J. Bard, L. R. Faulkner, J. Leddy and C. G. Zoski, *Electrochemical methods: fundamentals and applications*, Wiley New York, 1980.
117. A. Atkinson, *Journal of the Chemical Society. Faraday transactions*, 1990, **86**, 1307-1310.
118. K. Oura, V. Lifshits, A. Saranin, A. Zotov and M. Katayama, *Surface science: an introduction*, Springer Science & Business Media, 2013.
119. P. Heitjans and J. Kärger, *Diffusion in condensed matter: methods, materials, models*, Springer Science & Business Media, 2006.
120. S. Ruan, W. Zhang, Y. Sun, M. Ediger and L. Yu, *The Journal of Chemical Physics*, 2016, **145**, 064503.
121. W. Shockley, *Physical Review*, 1954, **93**, 345.
122. D. Kashchiev, *Nucleation: Basic Theory with Applications*, Butterworth-Heinemann, 2000.
123. J. E. McDonald, *American Journal of Physics*, 1962, **30**, 870-877.
124. D. W. Oxtoby, *Journal of Physics: Condensed Matter*, 1992, **4**, 7627.
125. X. Liu, *The Journal of Chemical Physics*, 2000, **112**, 9949-9955.
126. J. W. Mullin, *Crystallization*, Butterworth-Heinemann, 2001.

127. P. Cubillas and M. W. Anderson, *Zeolites and Catalysis: Synthesis, Reactions and Applications*, 2010, 1-55.
128. A. Myerson, *Handbook of industrial crystallization*, Butterworth-Heinemann, 2002.
129. F. Millange, M. I. Medina, N. Guillou, G. Férey, K. M. Golden and R. I. Walton, *Angewandte Chemie International Edition*, 2010, **49**, 763-766.
130. A. B. Albadarin, M. N. Collins, M. Naushad, S. Shirazian, G. Walker and C. Mangwandi, *Chemical Engineering Journal*, 2017, **307**, 264-272.
131. U. Pal, A. Sandoval, S. I. U. Madrid, G. Corro, V. Sharma and P. Mohanty, *Chemosphere*, 2016, **163**, 142-152.
132. J. Zhou, C. Tang, B. Cheng, J. Yu and M. Jaroniec, *ACS applied materials & interfaces*, 2012, **4**, 2174-2179.
133. L. Xiong, Y. Yang, J. Mai, W. Sun, C. Zhang, D. Wei, Q. Chen and J. Ni, *Chemical Engineering Journal*, 2010, **156**, 313-320.
134. S. Wang, M. Soudi, L. Li and Z. Zhu, *Journal of Hazardous Materials*, 2006, **133**, 243-251.
135. D. A. Fungaro, M. Bruno and L. C. Grosche, *Desalination and Water Treatment*, 2009, **2**, 231-239.
136. L. Li, S. Wang and Z. Zhu, *Journal of colloid and interface science*, 2006, **300**, 52-59.
137. S. Wang, H. Li and L. Xu, *Journal of colloid and interface science*, 2006, **295**, 71-78.
138. S. Wang, Y. Boyjoo, A. Choueib and Z. Zhu, *Water research*, 2005, **39**, 129-138.
139. N. Saad, M. Al-Mawla, E. Moubarak, M. Al-Ghoul and H. El-Rassy, *RSC Advances*, 2015, **5**, 6111-6122.